UNIVERSITY OF BIRMINGHAM

Characterising The Immune Environment in Metastatic Niches in Ovarian Cancer

By

Heba Awad Mohammed Sidahmed

A Dissertation submitted to the University of Birmingham for the degree of MASTERS OF SCIENCE BY RESEARCH

Institute of Immunology & Immunotherapy
College of Medical & Dental Sciences
University of Birmingham
April 2024

Abstract

Ovarian cancer (OvCa) continues to be a clinical challenge, with patients often presenting at late stage, and with a high occurrence of relapse and chemoresistance. The tumour microenvironment (TME) of the sites of metastasis in the omentum consists of a complex system of stromal, mesothelial, endothelial, and immune cells that echo the structure of secondary lymphoid organs and facilitate tumour spread and disease progression. This study aims to characterise the stromal cells in the TME, and further elucidate the immune-stromal interactions within the ovarian metastasis TME using C57BL/6J, DARE and IL-33 reporter murine models and human patient samples. Flow cytometry and Multiplex immunofluorescent microscopy were utilised in this study. PDPN-CD31- stromal populations expressing low amounts of FAP and CD140a are potential cancer-associated fibroblasts (CAFs) that may be involved in the direct progression of metastasis. There was also an increase in M1/M2 macrophages and cDC2 dendritic cells in metastatic omentum when compared to healthy omentum, parallel to an increase in cDC2 cells in DARE mice compared to the WT, which leads us to conclude that there is an increased immune activity within metastatic FALCs prior to chemotherapy, however more studies need to be conducted to determine if this activity is anti- or pro- high grade serous OvCa (HGSOC) tumoural proliferation.

List of Abbreviations

OvCa – ovarian cancer
HGSOC – high grade serous ovarian cancer
NACT – neoadjuvant chemotherapy
VEGF – vascular endothelial growth factor
NT – non-treated
FALC – fat-associated lymphoid cluster
TLO – tertiary lymphoid organ
SLO – secondary lymphoid organ
APC – antigen presenting cell
NK – natural killer (cell)
DC – dendritic cell
PDPN – podoplanin (Gp38)
FRC – fibroblastic reticular cell
LEC – lymphatic endothelial cell
BEC – blood endothelial cell
DN – double negative (cell)
TME – tumour microenvironment
IL – interleukin
G-CSF – granulocyte colony-stimulating factor
PAD4 – peptidyl arginine deiminase 4
NET – neutrophil extracellular trap
FGF – fibroblast growth factor
MMP – matrix metalloproteinase
FABP4 – fatty acid binding protein 4
scRNA-seq – single-cell RNA sequencing
IFN – interferon
TAM – tumour-associated macrophage
TNF – Tumour necrosis factor
WT – wild type
CAR – chimeric antigen receptor
PDL1 – programmed cell death ligand 1
HBRC – Human Biomaterials Resource Centre
BWH – Birmingham Women's Hospital
FC – flow cytometry
IHC – Immuno-histochemistry
SPF – specific pathogen-free
BMSU – Biomedical Services Unit
ITM – Institute of Translational Medicine
FFPE – formalin-fixed paraffin-embedded
FAP – fibroblast activation protein
ROI – region of interest
CAF – cancer-associated fibroblasts
αSMA - α-smooth muscle actin

List of Tables

List of Figures

Introduction

1. Ovarian Cancer Genesis and Metastasis

Ovarian cancer (OvCa) is a clinically challenging gynaecological malignancy arising from the ovaries or fallopian tubes. High Grade Serous OvCa (HGSOC), the most common type of OvCa, is epithelial in nature, and it is known to be typically diagnosed at later stages because of the silent progression of early disease, only becoming detectable after aggressive, wide-spread metastasis [1, 2]. This type of cancer is also known to display high rates of chemoresistance to conventional platinum- and taxane-based chemotherapies (e.g. cisplatin and paclitaxel respectively), even with debulking surgeries before chemotherapy (adjuvant) or following neoadjuvant chemotherapy (NACT). Treatment and management of OvCa is often dependent on time and resources, and while the most common pipeline involves surgical mass reduction, followed by chemotherapy and maintenance with drugs such as bevacizumab (a vascular endothelial growth factor (VEGF) inhibitor)[3], there is still debate on whether NACT reduces mortality compared to primary debulking surgery in NT (non-treated) patients, and the merits of adjuvant localised intraperitoneal vs systemic intravenous chemotherapy [4]. Most recent statistics in the UK report about 7,500 new cases of ovarian cancer diagnosed per year between 2016 and 2018, and a mortality rate of about 45% within five years of diagnosis [5]. Clinical biomarkers, such as CD47, are indicative of poorer prognosis (overall survival and progression-free survival) [6]. Most often than not, the patient will present with non-specific symptoms such as abdominal pain or swelling, which may be overlooked and misdiagnosed as a pathology of gastrointestinal origin. This is due to the transcoelemic path of metastasis that the primary tumour cells take after sloughing off the primary lesions, and due to the lack of anatomical barriers between the pelvic and abdominal cavities, the tumour cells are carried via peritoneal fluid to particular sites that support seeding of secondary tumours [1, 7, 8]. The main locus for OvCa metastasis is the greater omentum, an adipose-rich, double-layered peritoneal membrane extending from the greater curvature of the stomach and back up to the transverse colon, hanging before the intestines like an apron (figure 1) [9]. This highly vascularized organ has many functions, including localising inflammation, and providing a source of mesenchymal stem cells, stromal cells, and immune cells. Selective resection of the omentum (omentectomy) has been shown to limit the spread of OvCa and relapse with improved survival rates [9].

Within the adipose tissue of the omentum, there are many hubs of immune activity named fat-associated lymphoid clusters (FALCs), or milky spots, and they are classified as tertiary

lymphoid organs (TLOs) [10]. These FALCs were found to be the niches of metastatic seeding and disease progression [9]. The cell composition of TLOs is said to parallel that of secondary lymphoid organs (SLOs) such as lymph nodes, the tonsils, and thymus [11, 12] and contains a similar population of immune cells, including T and B lymphocytes, neutrophils, natural killer (NK) cells, macrophages, antigen presenting cells (APCs) and dendritic cells (DCs), providing innate and adaptive immunity. Other cells lending to the regulation of immune function, vascularisation, and structural integrity of the FALCs are epithelial, mesenchymal, and stromal cells, operating through an intricate and tightly coordinated network of cell-to-cell interactions [13, 14]. The stromal cells are further classified into four main subtypes that each serve a different function in maintaining homeostasis within the FALCs. They can be phenotypically classed by their expression, or lack thereof, of podoplanin (PDPN/GP38) and CD31. Fibroblastic reticular cells (FRCs, PDPN+CD31-) and lymphatic endothelial cells (LECs, PDPN+CD31+) support local DCs in antigen presentation to naïve T lymphocytes. Blood endothelial cells (BECs, PDPN-CD31+) promote the formation of high endothelial venules in SLOs and TLOs, which help the recruitment of lymphocytic organization into T- and B zones. Double negative (DNs, PDPN-CD31-) represent the largest subpopulation of stromal cells by far, and they are the least well-characterised subset [15]. Any of these immune or stromal cells, in isolation or combination, could provide possible targets for immunotherapy and are worth exploring to improve long term post-disease survival and limit relapse.

OvCa metastatic cells employ several mechanisms that evade these regulatory immune-stromal homeostatic conditions and stimulate angiogenesis to create a complex tumour microenvironment (TME). One such mechanism was demonstrated by Lee *et al*. wherein they showed that ovarian tumours support the aggregation of neutrophils in pre-metastatic FALCs by secreting interleukin (IL)-8, granulocyte colony stimulating factor (G-CSF), and other cytokines. The neutrophils then secrete peptidyl arginine deiminase 4 (PAD4), and form chromatin “webs,” referred to as neutrophil extracellular traps (NETs), which capture floating metastatic cells and embed them in the FALCs [16]. Neo-vascularisation is further prompted by the secretion of VEGF, fibroblast growth factor (FGF), and matrix metalloproteinases (MMP)-2 and -9 by the metastatic cells, and the adjacent mesothelial and mesenchymal stromal cells [1, 17]. The high adiposity of the omentum supplies the cancer cells with lipid stores to meet their high metabolic needs by β-oxidation through the expression of fatty acid binding proteins (FABP4) [1]. Jackson-Jones *et al*. in turn utilised single-cell RNA sequencing (scRNA-seq) on isolated omental murine CD45-CD41-Ter119-CD31-PDPN+/- stromal cells and identified a class of CXCL1+ mesothelial cells in the FALCs termed cover cells. In typical cases

of peritonitis, the expected course of events would be neutrophil aggregation and subsequent NET formation to entrap peritoneal debris and any sources of bacterial contamination. Jackson-Jones *et al*. were able to curb neutrophil recruitment in a murine model of zymosan-induced peritonitis by blocking CXCL1. In addition, inhibition of PAD4 also stopped the formation of NETs and the clearing of peritoneal contaminants [14].

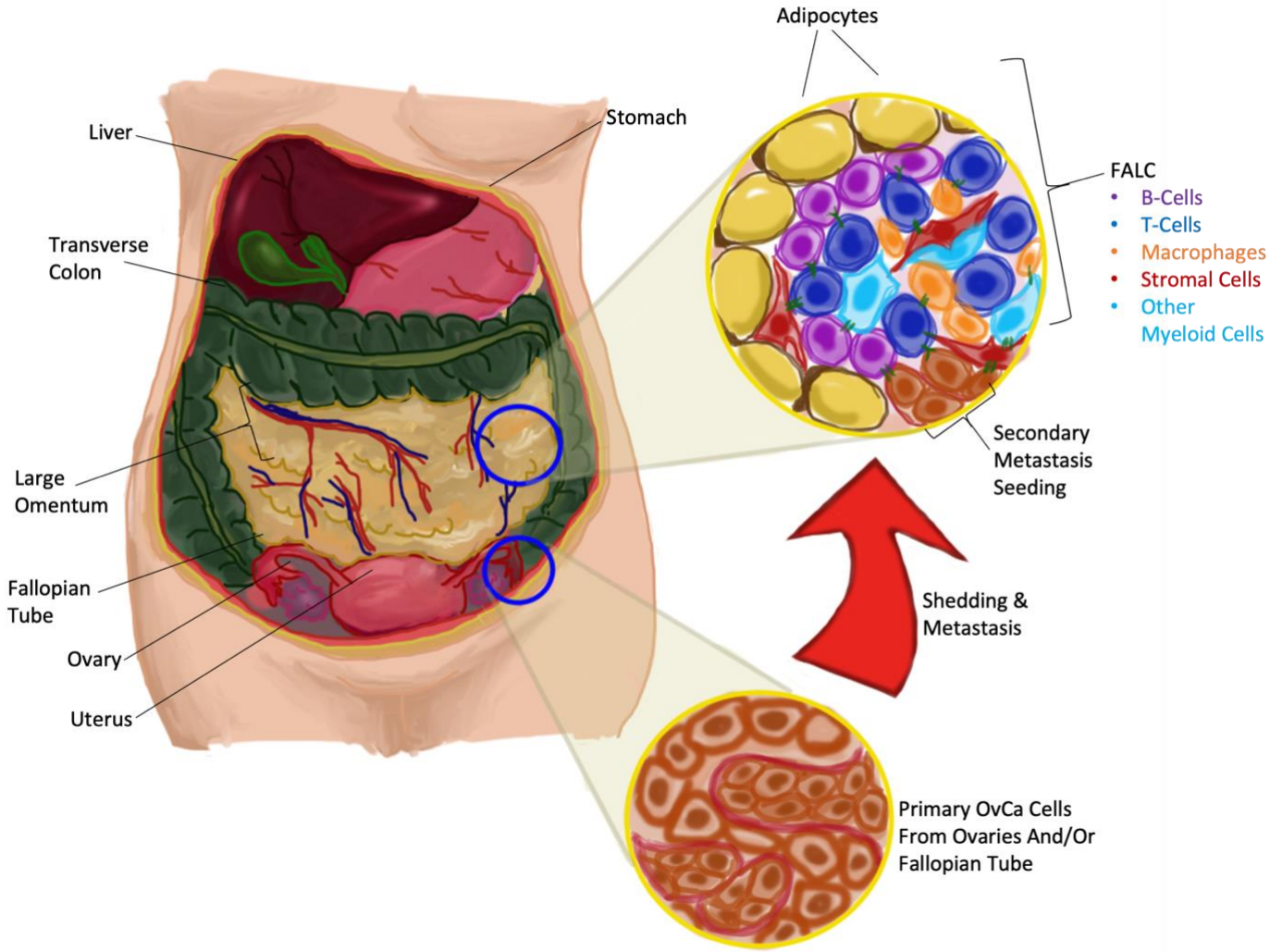

Figure 1. Pelvic and Abdominal Anatomy Facilitating OvCa Metastasis. Malignant cells from the ovaries and/or fallopian tubes travel through the peritoneal cavity to seed in FALCs found within the omental tissues. FALCs contain lymphoid and myeloid immune cells and stromal cells that interact with each other and facilitate metastasis and establishment of secondary tumours.

2. Experimental Approaches to Examine OvCa Metastasis

In a similar vein to the work of Jackson-Jones *et al*. and others [18], previous work from our group consisted of administering intraperitoneal injections of a colon cancer syngeneic cell line in C57BL6/6J mice which resulted in tumour formation in the mesenteric and omental FALCs and the formation of an immunosuppressive environment. Prophylactic induction of peritoneal inflammation prior to tumour cell injection led to a decrease in metastatic tumours, along with an increased number of interferon (IFN)-γ+ CD4 lymphocytes and NK cells, alluding to a means of curbing metastatic spread under a controlled and localised anti-tumour response. Moreover, more recent work from the group analysing the TME in primary ovarian and secondary metastatic tumours from ovarian cancer patients exhibited similar immunosuppression and the accumulation of Tregs and tumour associated macrophages (TAMs), in concordance with the syngeneic murine models.

An alternative to pharmaceutical induction of peritoneal inflammation, TNF-DARE (DARE) mice prove to be useful animal models, developing spontaneous and chronic inflammation. Heterozygous DARE mice, when bred, can produce either wild type (WT) or DARE phenotypes, allowing test animals to be compared with age-matched littermates, limiting other genetic variables that may skew results [19]. It is expected for omental and mesenteric FALCs of DARE mice to be larger, higher in number per unit weight, and contain more neutrophils than their WT counterparts, and they would be more readily capable to form NETs and entrap peritoneal contaminants [19, 20].

A promising alternative to pre-clinical animal models to study the cell-to-cell interactions within the TME is patient-derived organoids. It is a robust methodology with a success rate of 80% [21] and offers an accessible and time-efficient alternative to animal husbandry. Organoids can be cultured within 1-3 weeks after debulking surgery, regardless of whether the patient has received NACT or not [21, 22]. Additionally, organoids are genetically representative of intra-tumoural heterogeneity that is found within the patient [22, 23]. Co-culturing with tissue- or peripheral blood-derived immune cells, stromal, mesothelial and endothelial cells is also possible, and can provide a more accurate picture of patient response to various therapies, such as immune checkpoint inhibitors, specific chimeric antigen receptor (CAR) T cell therapy [21, 22], which can be of particular benefit to patients who have already developed resistances to conservative treatment.

3. Cellular Interactions Within the Metastatic Niche

The combined effect of stromal and immune cells in the metastatic niches shifts the phenotype of macrophages from a pro-inflammatory M1 to the immunosuppressive M2 phenotype, which further aids in malignant immune evasion [14, 24-26]. These tumour-associated macrophages (TAMs) are vital in omental metastasis in murine models, through the upregulation of the JAK-STAT signalling pathway [27]. Targeted depletion of these cells, especially the embryonically derived CD163+TIM+ subtype, significantly lowered the incidence of metastasis in experimental animal models when compared to the controls [16, 27, 28]. M1, M2 and M1/M2 (CD11c+CD206+) macrophages can all express programmed death ligand-1 (PD-L1), an immune checkpoint protein, and CD169 to recruit Tregs and interact with T and B lymphocytes [29]. CD169+ macrophages have also been described as positively prognostic in a few cancers [30-32].

A study by Louwe *et al*, also examined the origins of another subset of macrophages, CD102+, that can migrate from the peritoneum to the omentum following peritoneal inflammation [33]. While resident macrophages partially drive the infiltration of monocyte-derived macrophages, inflammatory macrophages could expand and repopulate the CD102+ and CD102- macrophage populations in the omentum, showing that origins of the macrophages have an impact on the immunogenic capacity following inflammation.

Another group [34] were able to show that the change in phenotype of TAMS from M1 to M2 plays a hand at promoting cisplatin resistance in ovarian cancer by the novel circRNA circITGB6, which was elevated in the serums of patients with cisplatin resistance. This molecule now has the potential to serve as therapeutic target and prognostic marker.

4. Aims and Hypothesis

4.1. Aims

1. Examine the presence and distribution of stromal and myeloid cells within healthy and metastatic omentum, centring on DCs, macrophages and neutrophils, using phenotypic characterization techniques such as flow cytometry and Multiplex immunofluorescent microscopy.
2. Elucidate the mechanisms through which the stromal and myeloid cells support the formation and sustaining of tumours.
3. Compare how the stromal and myeloid populations from human patient samples compare to the murine models of chronic inflammation.

4.2. Hypothesis

Ovarian cancer metastases gravitate towards omental FALCs and can influence the local immune environment to facilitate tumour growth.

Materials and Methods

All post-surgical patient samples were approved by and obtained through UoB's Human Biomaterials Resource Centre (HBRC application number **18-323** MetaFALC I - Deciphering the mechanism of metastasis formation in human peritoneal adipose tissues) and through a project specific ethical approval by Mr Jason Yap (HBRC and NHS REC **11-049** and IRAS **225991**). Retroactive formalin-fixed paraffin-embedded (FFPE) samples were obtained from Birmingham Women's Hospital (BWH).

This project used the same ethical approvals as it was a continuation of the aforementioned project.

1. Murine Models and Tissue Preparation

1.1 Murine Models

C57BL/6J, DARE and IL-33 reporter murine strains were bred and housed under specific pathogen free (SPF) conditions in the UoB Biomedical Services Unit (BMSU) and underwent humane culling by cervical dislocation. When some IL-33 reporter mice were nearing their culling date and would otherwise be unutilised, they were made available to us by the BMSU, and they were used as an additional control (non-inflammatory model).

1.2 Murine Tissue Preparation

The relevant fatty tissues (omentum and mesenteries) and mesenteric lymph nodes (mLN) were collected, weighed, and finely chopped prior to digestion in the appropriate enzymatic mixture. The fatty tissues were processed in a mixture of DNAse I (10 mg/ml stock, 1:100), collagenase P (100 mg/ml stock, 1:500) and collagenase dispase (100 mg/ml stock, 1:125) [all obtained from Roche, Merck Life Sciences] in 2% fetal calf serum (FCS) RPMI [both from Gibco] at 37^{o}C for a duration of 30 minutes with continuous agitation. mLNs were either a) pierced with a sterile needle and placed into 1 mL micro vials with a digestion mixture of collagenase dispase and DNAse I at 37^{o}C for 30 minutes to target myeloid cells, or b) roughly chopped with scissors and digested with DNAse I (1:50) and collagenase D (100 mg/ml stock, 1:40) [Roche, Mercke Life Sciences] in serum-free RPMI at 37^{o}C for 35-60 minutes to target stromal cells. 0.5M EDTA was added to stop the digestion, and the cells were collected and filtered through a 70 μm filter for antibody staining and FC acquisition. The panels are outlined in tables 1-2.

2. Human Tissue Preparation

Ovarian and omental samples from tumours and/or uninvolved tissues were obtained from NT and NACT patients who had signed written informed consent (BCH). During transport, the samples were stored in 2% FCS RPMI. Tissues were then portioned (up to 0.8 g) and as per the protocol used for murine fatty tissues mentioned above. Cold 2% FCS RPMI was used to stop digestion, and the cells were strained through a 70 μm filter. The panels for extra- and intracellular staining are stated in tables 3-5.

3. Tissue Staining Panels and Phenotyping Characterization

Murine and human tissues were stained using the antibody panels detailed in tables 1-5. The cells were acquired with LSR Fortessa and the FACSDiva acquisition software [BD Biosciences].

Marker	Function	Cell Subtype	Dilution	Cat. No.	Supplier
CD45.2	Hematopoietic cell marker	Hematopoietic cells	1:300	109841	Biolegend
CD3	Lymphoid cell markers	T cells	1:300	553062	BD Biosciences
B220		B cells	1:200	557957	BD Biosciences
CD11b	Myeloid identification markers	cDC2	1:200	17-0112-83	eBioscience
Ly6g		Neutrophils	1:300	127616	Biolegend
SiglecF		Eosinophils	1:200	562681	BD Biosciences
Ly6C		Macrophages	1:800	128017	Biolegend
MHC II		DCs	1:600	107635	Biolegend
CD11c			1:300	117336	Biolegend
CD103		cDC1	1:200	12-1031-81	eBioscience

Table 1. Murine - Myeloid characterisation markers.

Marker	Function	Cell Subtype	Dilution	Cat. No.	Supplier
CD45.2	Hematopoietic cell markers	Hematopoietic cells	1:200	109839	Biolegend
Ter119		Erythroid cells	1:1000	45-5921-80	eBioscience
Gp38	Stromal cell marker	Stromal cells	1:100	127411	Biolegend
CD31	Endothelial cell marker	Endothelial cells	1:200	48-0311-82	eBioscience
CD29	Adhesion molecules	Epithelial and stem cells	1:400	17-0291-80	eBioscience
CD44		Stromal and stem cells	1:200	103059	Biolegend
CD106/VCAM-1		Mesenchymal stromal cells	1:200	11-1061-82	Invitrogen

Table 2. Murine - Stromal cell characterisation markers.

Marker	Function	Cell Subtype	Dilution	Cat. No.	Supplier
CD45	Hematopoietic cell marker	Hematopoietic cells	1:300	304047	Biolegend
CD3	Lymphoid cell markers	T cells	1:300	300463	
CD19		B cells	1:300	302245	
CD56		NK cells	1:300	362542	
CD11c		DCs	1:200	301604	

HLA-DR/MHC II	Myeloid identification markers	DCs	1:200	307636	
CD14		Monocytic/inflammatory DCs	1:200	325631	
CD141		cDC1	1:200	344110	
CD1c		cDC2	1:200	331533	
XCR1		Migratory DCs	1:200	372605	
CD86	Activation markers	DCs	1:300	305427	
CCR7			1:200	353223	
PD-L1	Immune inhibition protein		1:200	329705	

Table 3. Human - Myeloid/dendritic cell characterisation markers.

Marker	Function	Cell Subtype	Dilution	Cat. No.	Supplier
CD45	Hematopoietic cell marker	Hematopoietic cells	1:300	304035	Biolegend
CD3	Lymphoid cell markers	T cells	1:400	300463	
CD19		B cells	1:300	302245	
CD56		NK cells	1:300	362542	
HLA-DR/MHC II	Myeloid identification markers	Non-lymphoid cells	1:200	307636	
CD11b		Neutrophils and macrophages	1:200	101237	
CD66b		Neutrophils	1:200	305113	
CD163		M2 macrophages	1:100	333627	
CD11c		M1 macrophages	1:200	301604	
CD86	Activation markers	Macrophages	1:200	305427	
CD169			1:100	346013	
Ki-67	Proliferation marker		1:100	350513	
PD-L1	Immune inhibition protein		1:100	329705	

Table 4. Human - Myeloid/macrophage characterisation markers.

Marker	Function	Cell Subtype	Dilution	Cat. No.	Supplier
CD45	Hematopoietic cell marker	Hematopoietic cells	1:300	304035	Biolegend
CD235a/Glycophorin A	Erythrocyte marker	Erythroid precursors and erythrocytes	1:100	349105	
CD31	Endothelial adhesion molecule	BECs and LECs	1:300	303135	
Podoplanin (PDPN/Gp38)	Cellular motility glycoprotein	FRCs	1:300	337021	
Fibroblast Activation Protein (FAP)	Activation and proliferation induction	Fibroblasts and CAFs	1:200	FAB3715N	Bio-Techne
CD140α/PDGFRα	Growth factor receptor	Stromal fibroblasts	1:200	562799	BD Biosciences
Ki-67	Proliferation marker	Actively proliferating cells	1:50	556026	
IL-33	Th2 cytokine inducer	Stromal fibroblasts	1:50	10368-MM03-F	Sino Biological

Table 5. Human - Stromal characterisation markers.

4. Multiplex Immunofluorescent (IF) Staining and Microscopy

FFPE retrospective metastatic omental and/or primary ovarian samples from 10 patients were acquired (Dr. Raji Ganesan, BWH). Paired samples were used when available to compare primary and secondary tumours. Slide preparation and staining was carried out at the Institute of Translational Medicine (ITM, UoB, Queen Elizabeth Hospital) using the UltiMapper I/O Immuno8 Kit [Ultivue]. The pre-set panel is outlined in table 6. Multiplex IF images were acquired by the Vectra Polaris Microscope. The images were digitally pre-processed by overlapping the DAPI nuclear stain channels to produce composites that were viewed and quantitatively analysed on the VisioPharm software platform and GraphPad Prism 10.

Marker	Function	Cell Subtype
CD3	T Lymphocyte activation marker	T lymphocytes
CD4	T cell co-receptor	Helper T cells
FOXp3	Regulatory transcription factor	Tregs
CD8	T cell co-receptor	Cytotoxic T cells
CD68	Myeloid lineage marker	Macrophages
CK-Sox10	Epithelial cell marker	Some OvCa tumours
PD1	Immune inhibition receptor	CD3/4/8 cells
PD-L1	Immune inhibition protein	Macrophages and tumour cells

Table 6. Ultivue multiplex IF panel.

5. Statistical Analysis

After flow cytometry data acquisition and analysis in FlowJo v10.8.1, statistical data was initially sorted on Microsoft Excel and analysed on GraphPad Prism 9 and Prism 10. Statistical significance was calculated by the Mann-Whitney test when comparing two groups, and the Kruskal-Wallis one-way ANOVA test when analysing two or more variables. The Chi-squared test was used when comparing un-paired proportions of cell populations. Statistical significance is denoted by *$p<0.05$, **$P<0.01$, and ***$P<0.001$. p values were not indicated for non-significant data (ns).

Results

1. Murine WT vs DARE FC Data

Flow cytometry analysis of select murine SLOs (mesenchymal lymph nodes) and TLOs (FALCs present in the omentum and mesentery) was performed to characterise their immune and stromal populations, and to compare the variation in proportions of these populations between different murine strains. DARE mice were selected for their chronic inflammatory status, which leads to an increased number of more populous FALCs when compared to their WT littermate controls. As previously mentioned, inflammatory conditions in the peritoneum may lead to an anti-tumoural environment. We would like to examine in which immune and stromal subpopulations do the DARE TLOs differ from their WT counterparts, and if this will help us predict metastatic behaviours in future cancer experimental models. IL-33 reporter mice were used on some experimental runs when the mice in question were to be otherwise culled and discarded by the BMSU. These mice were tested to examine how similar, or dissimilar their immune and stromal populations are to WT and DARE mice.

1.1 Murine Stromal FC Analyses

Omental and mesenteric tissues provided usable data to observe stromal cells. Viable CD45.2-Ter119- cells were sorted into FRCs, LECs, BECs, and DNs according to Gp38/podoplanin and CD31 expression, stromal and endothelial markers respectively. mLNs were not quantitatively adequate for statistical analysis due to low viability upon FC acquisition and were majority DNs in both WT and DARE mice (59.1% vs 84.4% respectively, 2A). DARE mesenteries in comparison to those of WT mice are generally smaller and less vascularised, appearing atrophied, and yielding smaller cell pellets post enzymatic digestion. Despite this, in the mesenteric stromal populations, there were no significant differences between WT and DARE mice, however when IL-33 reporter mice were compared, WT mice had a bigger population of DNs and a smaller population of BECs (figure 2B-C). In contrast, while the gross stromal population was more numerous in WT mice than DARE mice, their subpopulation proportions were comparable. IL-33 reporter mice also had a much higher proportion of FRCs than DARE mice (figure 2D-E).

1.2 Murine Myeloid FC Analyses

In the myeloid compartments, monocytes were the predominant CD11b+ subtype in the lymph nodes of WT and DARE mice, with no significant differences in the proportion of eosinophils. Macrophages, on the other hand, appear to be more highly present in the lymph nodes and omental tissues of DARE mice. This trend is also seen in the mesenteric myeloid populations, except for a higher eosinophil proportion observed in the WT (figure 3).

Figure 4A-C shows the proportions of DCs in the mLNs and omental tissues, and the WT mesentery. There is a decrease in the DARE lymph nodes compared to the WT samples, while the opposite can be seen in the omental tissues. cDC2s are the prevalent subtype of DCs in most of the samples, and there is a significantly number of cDC2s in DARE omentum compared to the WT. Varying amounts of CD103+CD11b+ DCs are present in the samples, particularly in the lymph nodes.

1.3 Murine Lymphoid FC Analyses

When examining the lymphoid cells in the mLN and omentum, CD8 cells were markedly increased in the mLN of DARE mice (figure 5A), but no significant difference was seen in the Omentum (figure 6A). iNKT, CD8 and CD4 were selectively re-stimulated with a combination of PMA (100μg/ml stock in DMSO), Ionomycin (1mM stock in DMSO), BFA (5m/ml, Biolegend) and Golgi stop and incubated for 3 hours at 37^{o}C 5% CO_2. Unstimulated controls were incubated with only BFA, and Golgi stop. While there was an increased activity in re-

stimulated CD4 IL10+ and CD8 IFNγ+ in mLN WT mice (figure 5B, F), this corresponding increase was only seen in the DARE mice in omental tissues (figure 6B, F).

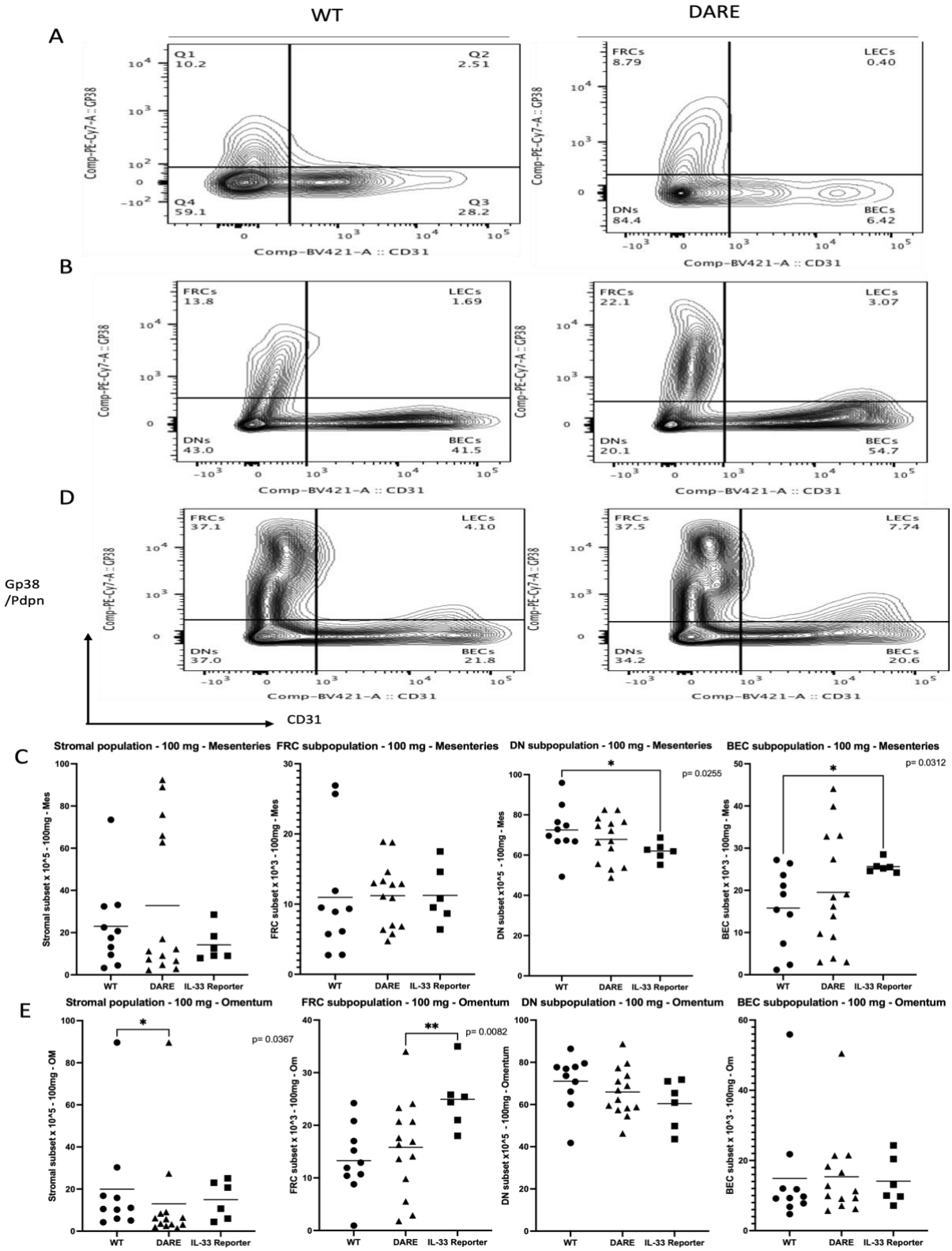

Figure 2. Representative stromal FC analysis of WT, DARE and IL-33 reporter mice. A, B, D) mLN mesenteric and omental respectively. Populations: Q1) Gp38+CD31- fibroblastic reticular cells (FRCs), Q2) Gp38+CD31+ lymphatic endothelial cells (LECs), Q3) Gp38-CD31+ blood endothelial cells (BECs), Q4) Gp38-CD31- double negative stromal cells (DNs). C) Gross population and subpopulations of mesenteric stromal cells normalised to 100mg tissue. E) Gross population and subpopulations of omental stromal cells normalised to 100mg tissue. Mann-Whitney test where significance was found; p-values are indicated in the figures.

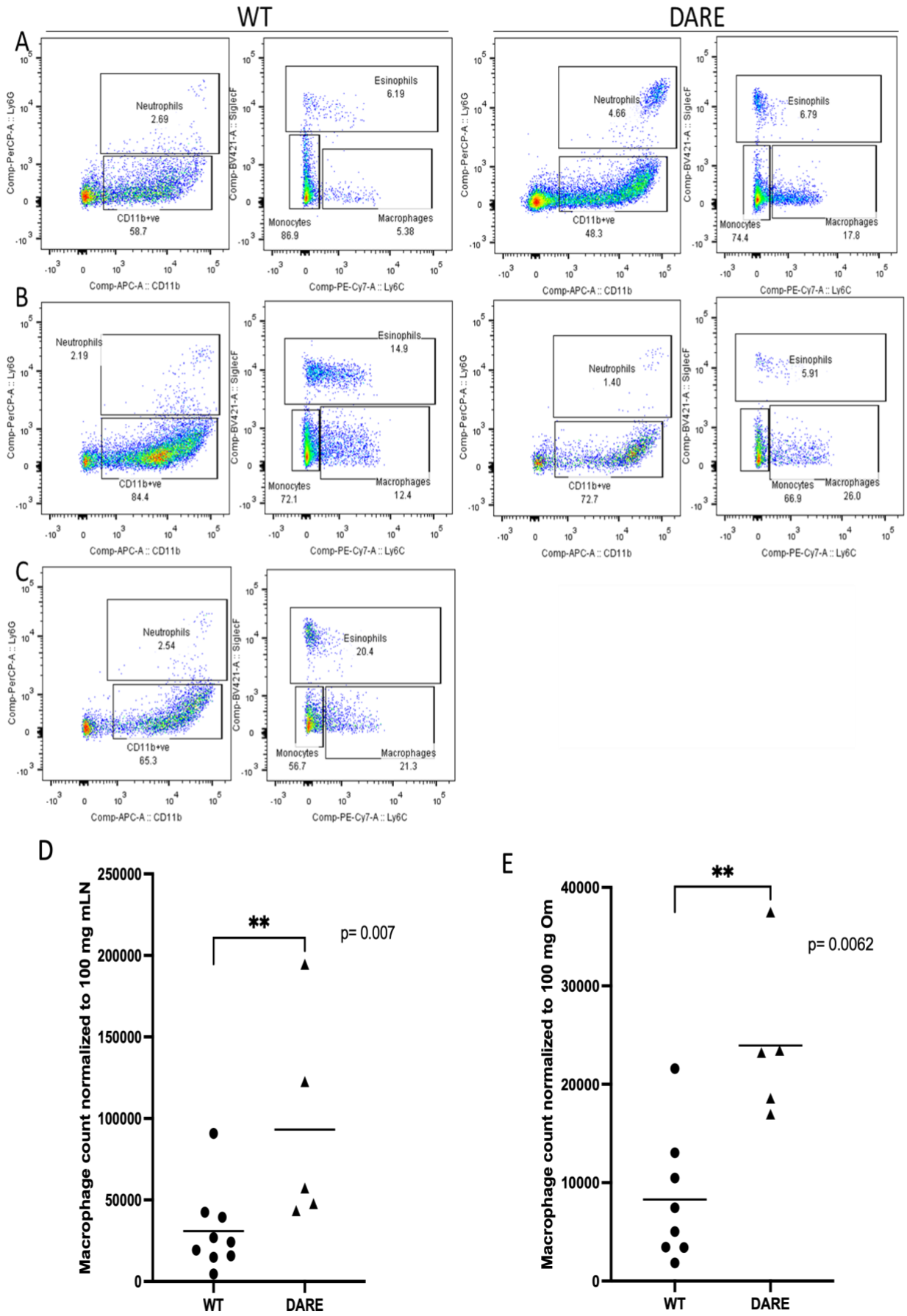

Figure 3. Analysis of myeloid populations of wild-type and DARE littermates. A) Mesenteric lymph nodes. B) Omentum. C) Mesenteries. D) mLN macrophages normalised to 100mg tissue. E) Omental macrophages normalised to 100mg tissue. Mann-Whitney test for statistical significance; p-values indicated where there is significance.

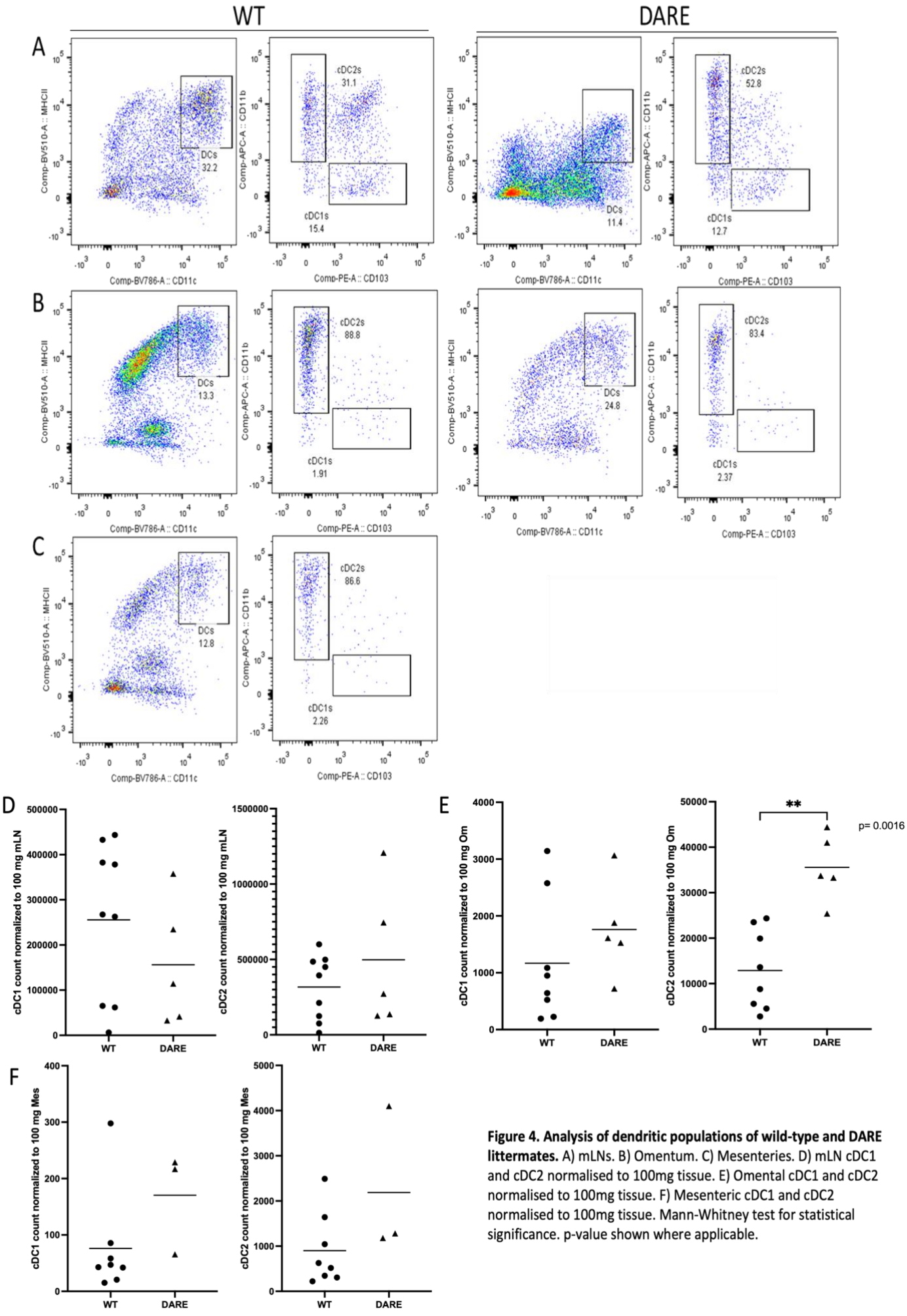

Figure 4. Analysis of dendritic populations of wild-type and DARE littermates. A) mLNs. B) Omentum. C) Mesenteries. D) mLN cDC1 and cDC2 normalised to 100mg tissue. E) Omental cDC1 and cDC2 normalised to 100mg tissue. F) Mesenteric cDC1 and cDC2 normalised to 100mg tissue. Mann-Whitney test for statistical significance. p-value shown where applicable.

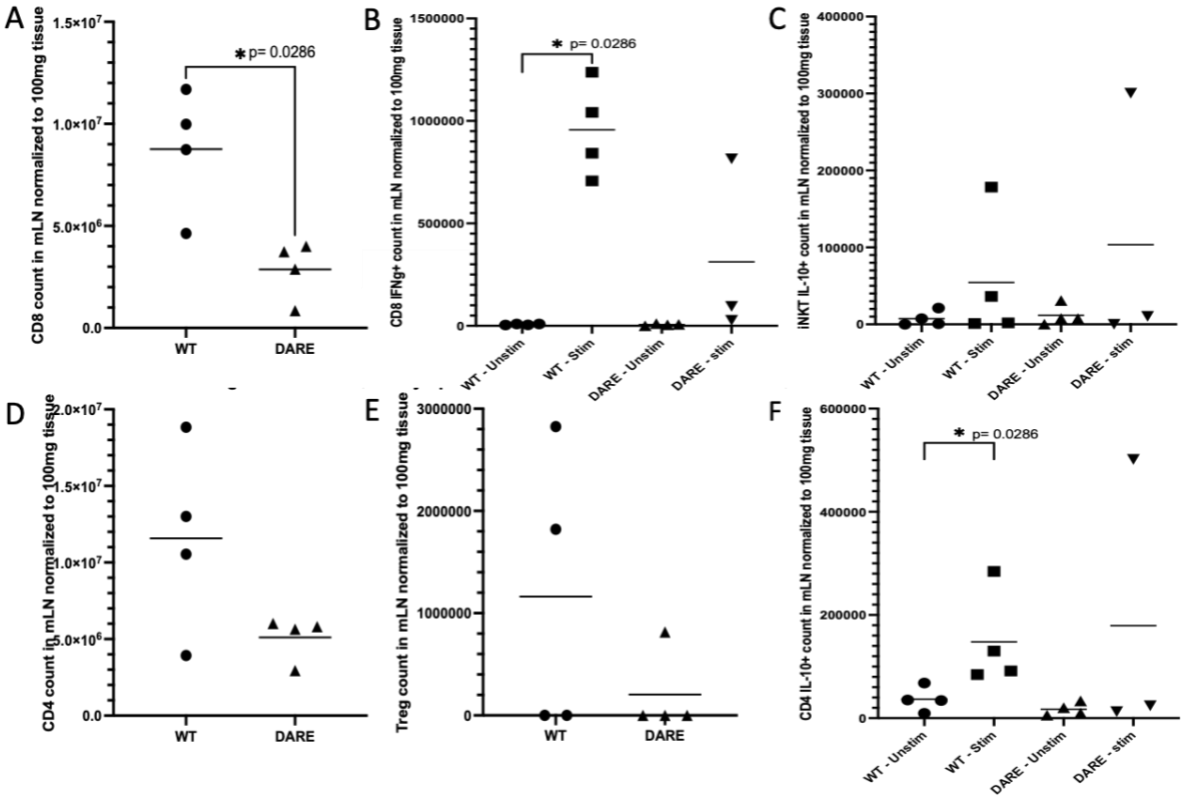

Figure 5. mLN Lymphoid populations in WT vs DARE mice, normalised to 100mg tissue. A) CD8 T cells. B) CD8 IFNγ+ in WT and DARE samples +/- re-stimulation with PMA/Ionomycin mix. C) iNKT cells in WT and DARE samples +/- re-stimulation with PMA/Ionomycin mix. D) CD4 T cells. E) Tregs. F) CD4 IL10+ in WT and DARE samples +/- re-stimulation with PMA/Ionomycin mix. Mann-Whitney test for statistical significance.

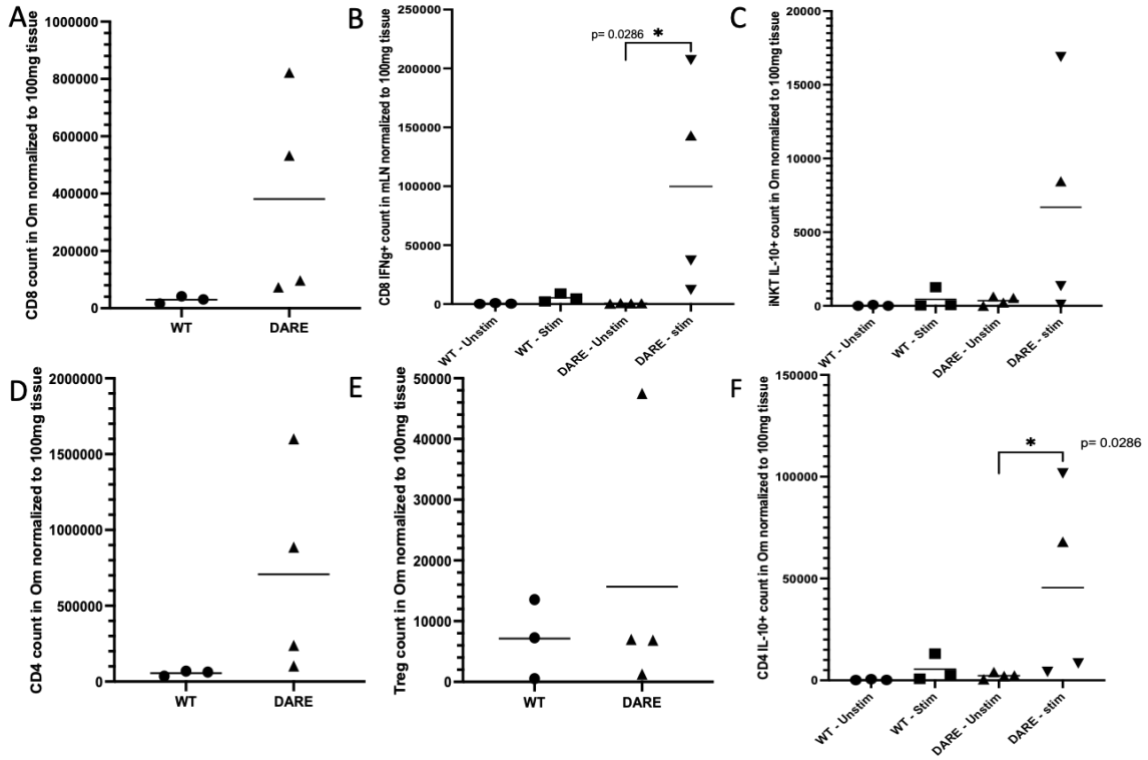

Figure 6. Omental lymphoid populations in WT vs DARE mice, normalised to 100mg tissue. A) CD8 T cells. B) CD8 IFNγ+ in WT and DARE samples +/- re-stimulation with PMA/Ionomycin mix. C) iNKT cells in WT and DARE samples +/- re-stimulation with PMA/Ionomycin mix. D) CD4 T cells. E) Tregs. F) CD4 IL10+ in WT and DARE samples +/- re-stimulation with PMA/Ionomycin mix. Mann-Whitney test for statistical significance.

2. Human Samples FC Findings and Analysis

Samples from NT patients were collected during initial staging procedures before any medical intervention or management is administered; therefore, the samples give us a baseline for the myeloid and stromal populations in the patient's primary and secondary tumours and/or uninvolved omental tissues. On the other hand, NACT patients had at least 1 round of chemotherapy, and were admitted for debulking surgeries to remove most of their remaining visible tumours after medical intervention. FC analysis was conducted to examine the effect of chemotherapy on the immune and stromal subpopulations found within and around the tumours. Ideally, NT patients would be followed up on a long-term basis, with more samples collected from them when they undergo post-NACT debulking surgeries, to directly observe the cellular subpopulation changes. This should also be paired with whole-mount and IHC microscopy to supplement FC analysis results.

2.1 Immune subpopulations in NT vs NACT patients

The myeloid and dendritic cell populations from healthy human omentum and the metastatic omentum of NT and NACT HGSOC patients were compared (figures 7-8 respectively). Relatively small neutrophil populations were observed in the NACT metastatic omentum. Macrophages skewed towards an M2 phenotype in healthy and NT omental tissues (figure 7). The M1/M2 (CD11c+CD206+) population was also significantly higher in metastatic omentum, despite having smaller numbers overall when normalised to 100mg of tissue. Compared to the healthy omentum, the omentum with metastasis had a higher proportion of DCs, $CD14^{+}$ inflammatory DCs, cDC2s and migratory DCs (figures 8-9).

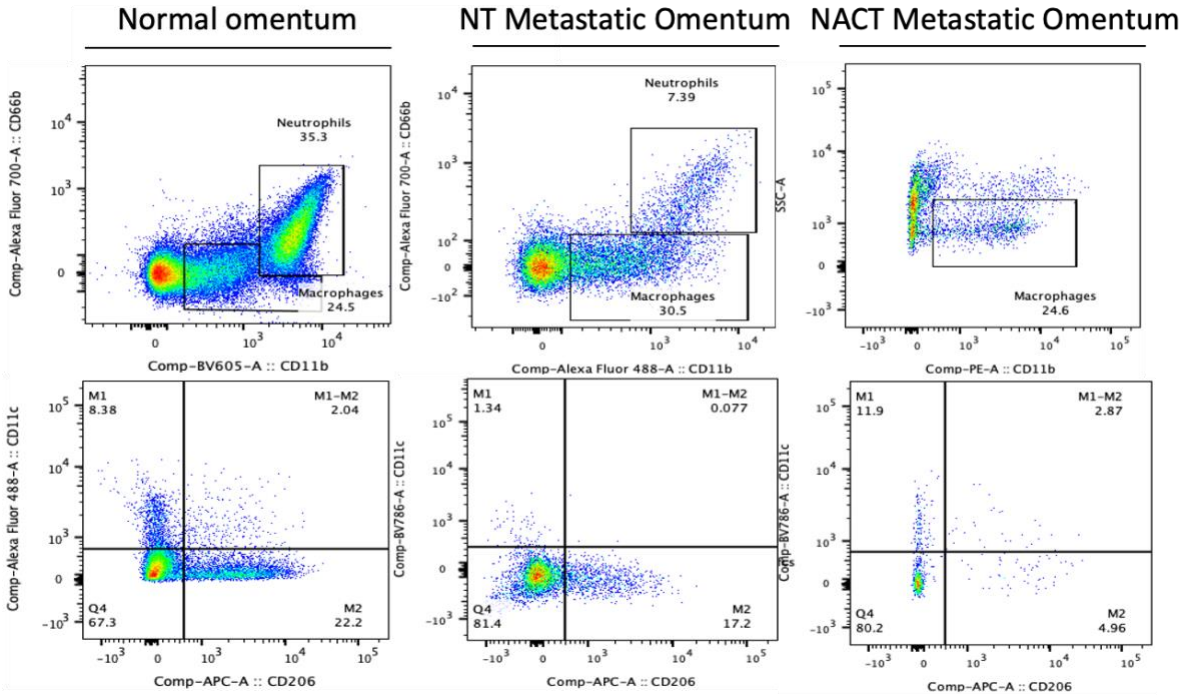

Figure 7. Representative FC data of normal, NT and NACT metastatic omentum. Macrophages were gated on the CD11b+CD66b- population and classified into M1 and M2 using CD11c and CD206. The shift from a predominantly M2 phenotype in normal and NT metastatic omentum to the pro-inflammatory M1 in NACT metastatic omentum can be interpreted to be the formation of an anti-tumoral response.

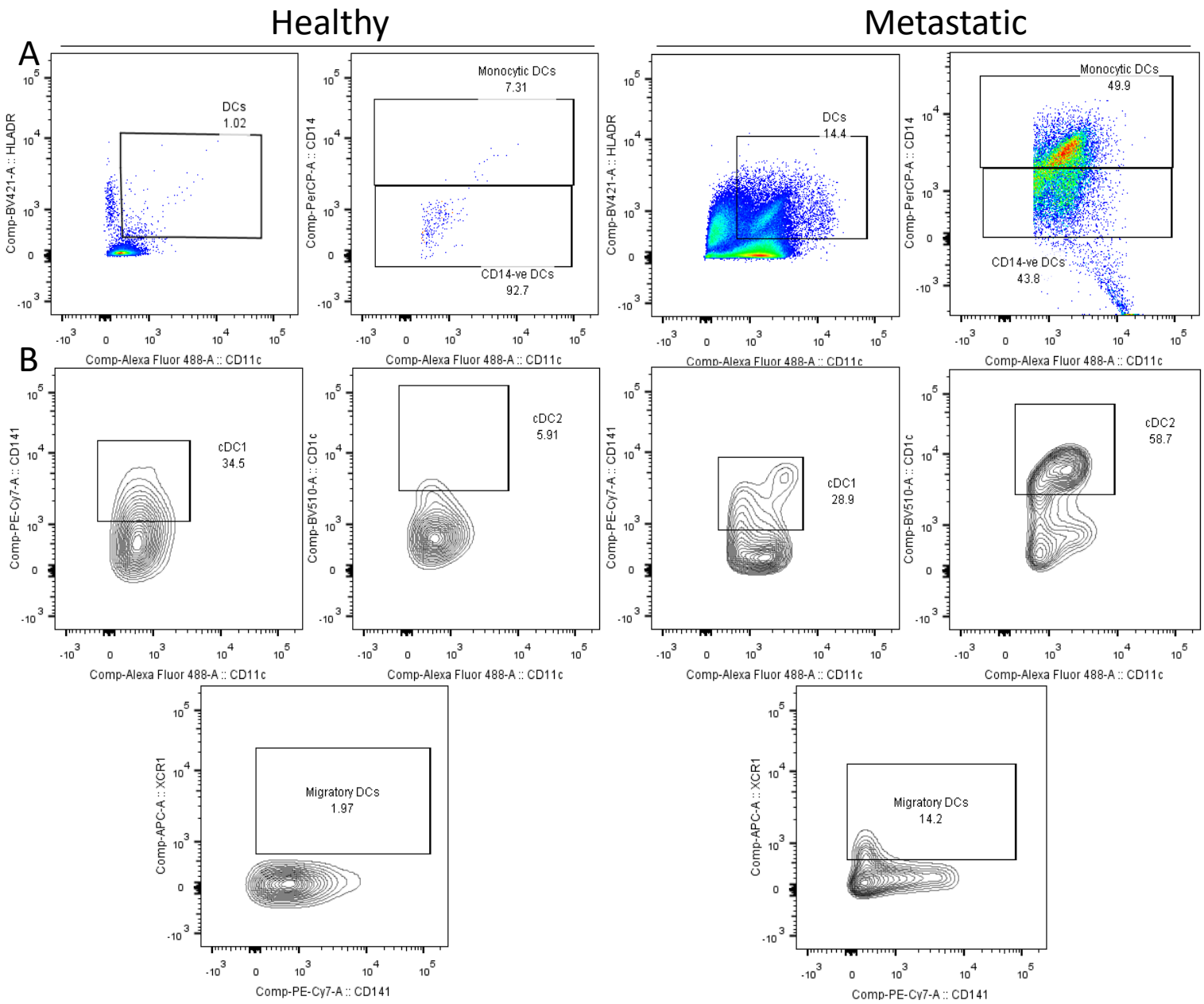

Figure 8. Analysis of dendritic cell populations in omental samples from a healthy control and a HGSOC patient carrying metastases. A) Total DCs, monocytic/inflammatory and CD14^{-} distributions. **B)** Subsets of CD14^{-} DCs: cDC1, cDC2 and migratory DCs.

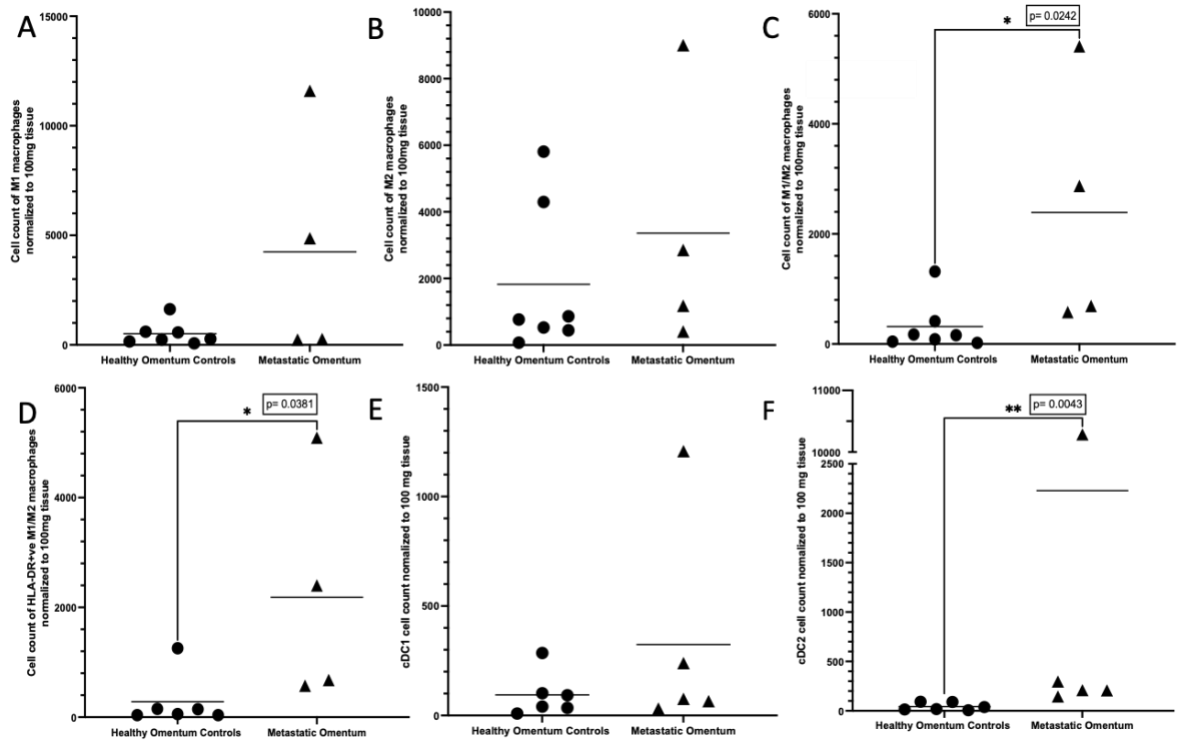

Figure 9. Omental myeloid and dendritic populations in healthy vs metastatic omental tissues, normalised to 100mg tissue. A) M1 macrophages B) M2 macrophages. C) M1/M2 macrophages D) M1/M2 HLA-DR+ macrophages. E) cDC1. F) cDC2. Mann-Whitney test for statistical significance.

2.2 Human Stromal subpopulations in NT vs NACT samples

FC data of stromal populations characterised by CD45-CD235a-PDPN+/-CD31+/- were also examined for FAP and CD140a/PDGFRα expression (figure 10). In our sample cohort, the majority of FAP^{lo} CD31- cells were DN stromal cells, and subsequent gating showed that these cells are also typically negative or have a low expression of CD140a (figure 10A). Conversely, whilst the FRCS also lacked in substantial expression of CD140a, they mostly displayed an intermediate-high expression of FAP (typically ≥50% proportion of FAP+ FRCs).

Another mechanism through which stromal cells regulate immunity is the expression of IL-33, which in turn promotes the synthesis of T_h2 cytokines and the activation of group 2 innate lymphoid cells (ILC2s). This causes FALC expansion and recruitment of inflammatory monocytes and neutrophil migration to the peritoneal cavity. The numbers of IL-33-expressing stromal cells within our cohort is shown in figure 11.

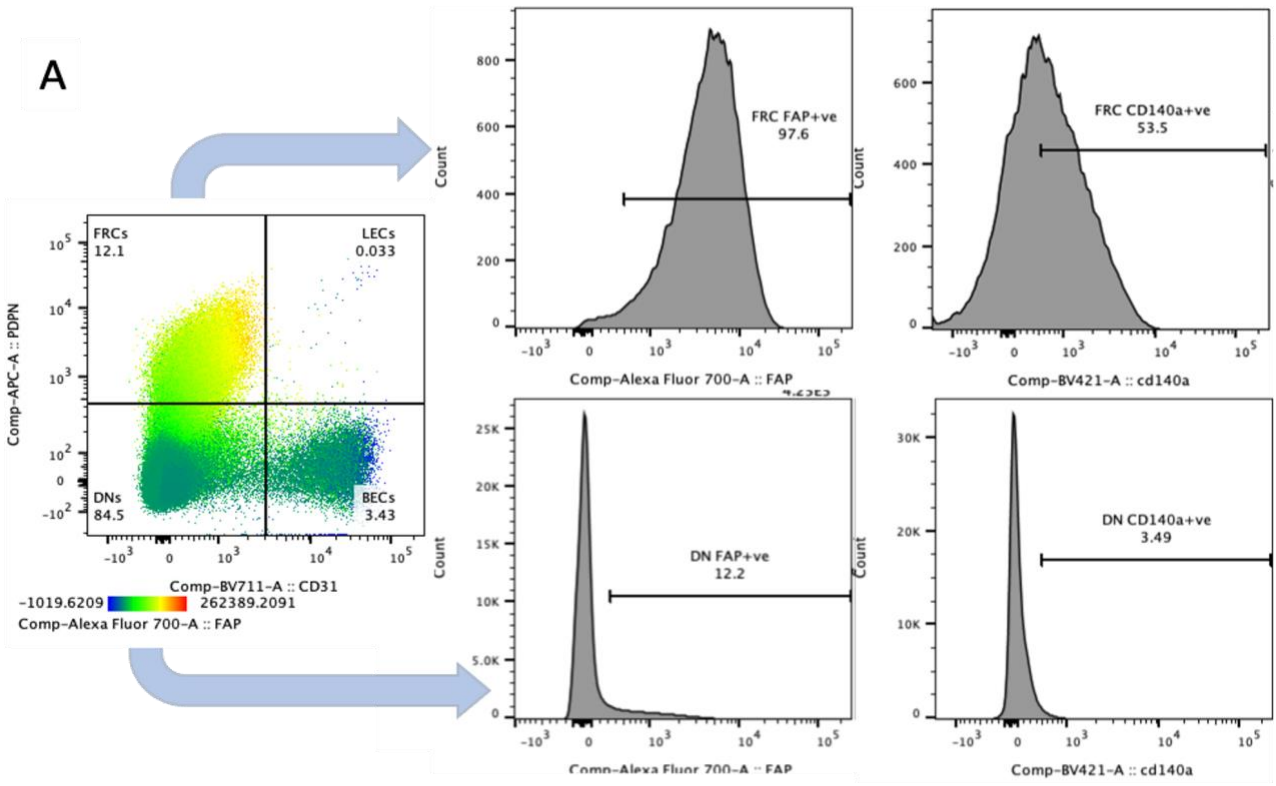

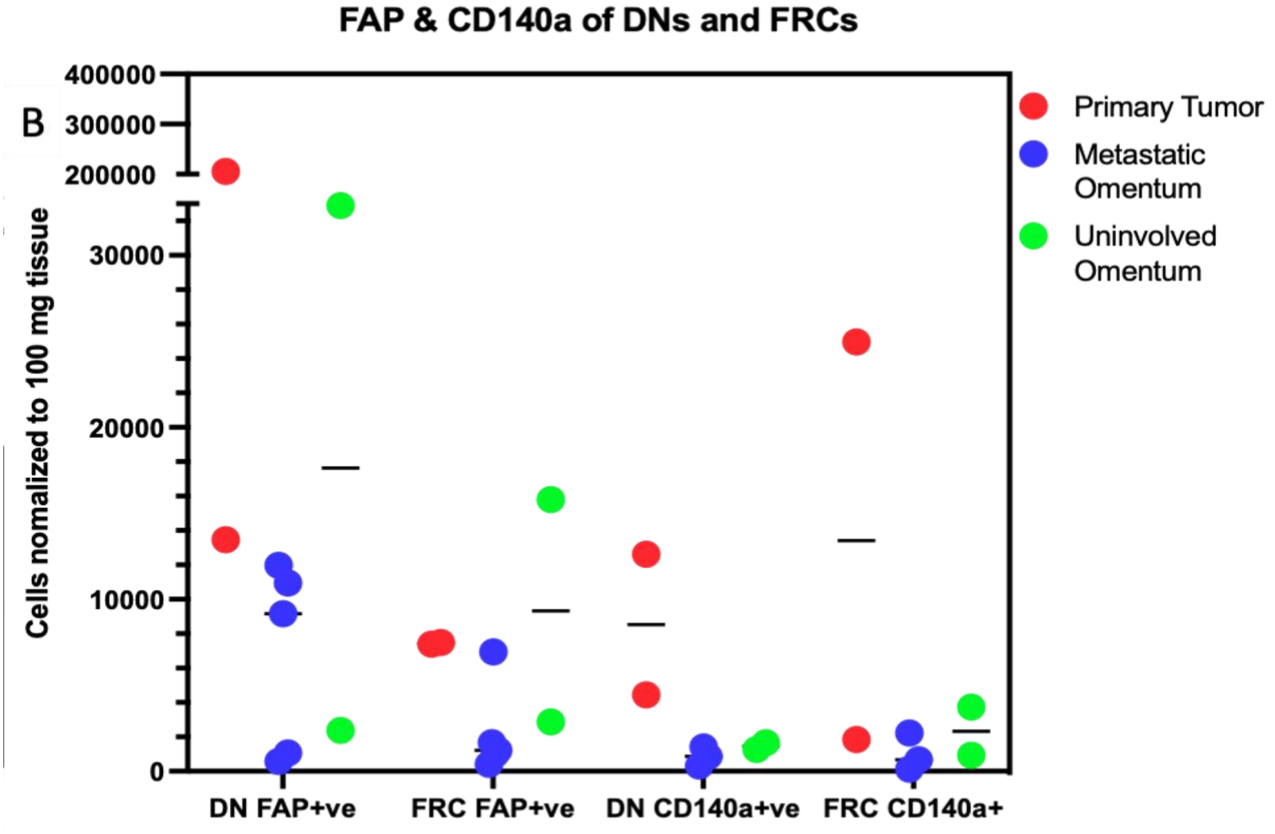

Figure 10. Stromal population expression of FAP and CD140a/PDGFRα in FRCs and DNs. A) Representative FC data of the proportion distribution of stromal subtypes in our OvCa samples, and the proportion of FAP+ FRCs and DNs, and CD140a+ FRCs and DNs. B) The number of these cell subtypes normalized to 100 mg of tissue. There was no significant statistical difference between the averages of the primary tumors, metastatic and uninvolved omentums with the one-way ANOVA test (p=0.22).

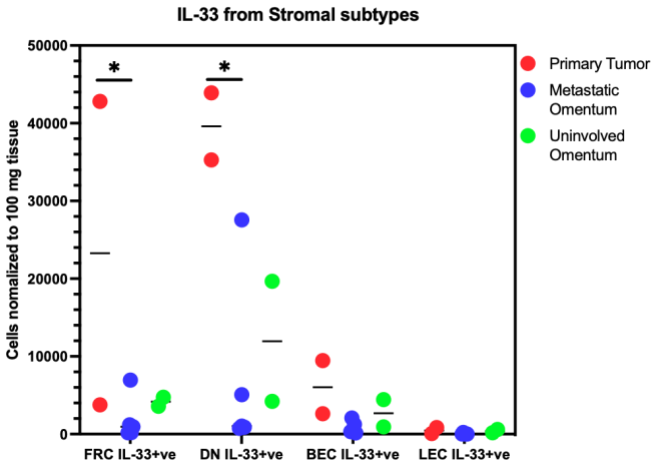

Figure 11. IL-33 expressing cells across different stromal subtypes and different tissues. Normalised cell counts to 100 mg of tissue show that the FRCs and DNs include the biggest proportions of IL-33+ cells. FRCs and DNs from primary ovarian tumors are more likely to express IL-33 than their counterparts in metastatic and uninvolved omental tissues ($p<0.05$, Chi-square test). Interestingly, while LECs were the least frequent population amongst all tissues in number and proportion, they had the highest IL-33 expression in terms of MFI.

3. IF Microscopy Supports Human FC Findings

IF microscopy was an important tool that allowed us to examine the primary and metastatic niches of OvCa and localise the sites of metastasis in relation to the immune infiltrate found within the FALCs of the omentum. Unlike the disruptive process of digestion and sample preparation for FC, examining FFPE samples allows us to closely examine the physical proximity of immune and tumoural cells, and to also compare the tumoural load between NT and NACT samples. While there were challenges and limitations in slide preparation due to cost and the physical properties of the omental samples, we aimed to observe the proportion of immune infiltrates, tumoural load, phenotypes and compare them to the FC data of these patients that was previously acquired. While the pre-made panel provided promising results, in the future, additional markers for identifying B cells and stromal cells should be accounted for to have more comprehensive results.

3.1 Localisation and Visualisation of OvCa Tumours in Ovaries and FALCs

A total of 10 patients provided either NT or NACT omental and/or ovarian samples as FFPE preparations (summarised in table 7). After acquisition and primary processing of microscopy images (figure 12), native nuclear detection applications on VisioPharm were used to quantify the cells within regions of interest (ROIs) that were designated as either tumour or uninvolved tissue, using H&E-stained slides of the same patient samples provided by Dr. Raji Ganesan (BWH) as references. Due to limitations of VisioPharm software in capturing all the cells that would be positive for an individual stain (e.g., all CD68+ cells), several markers had to be combined for the cells to be detectable (e.g., combining CD68, CD4, and PDL1 to achieve a clear view of all CD68+ cells). Initial imaging compared the localised immune clusters found in the omental tissues, proximal to CK-SOX10+ tumour cells, to standardised tonsil samples,

as these cells were possible FALCs, and therefore should mirror the SLO structures found within the tonsils (figure 13).

Following quantification of staining data, custom application algorithms were programmed and implemented to compare the phenotypic profiles of the samples (figures 14-15 for omental and ovarian samples respectively).

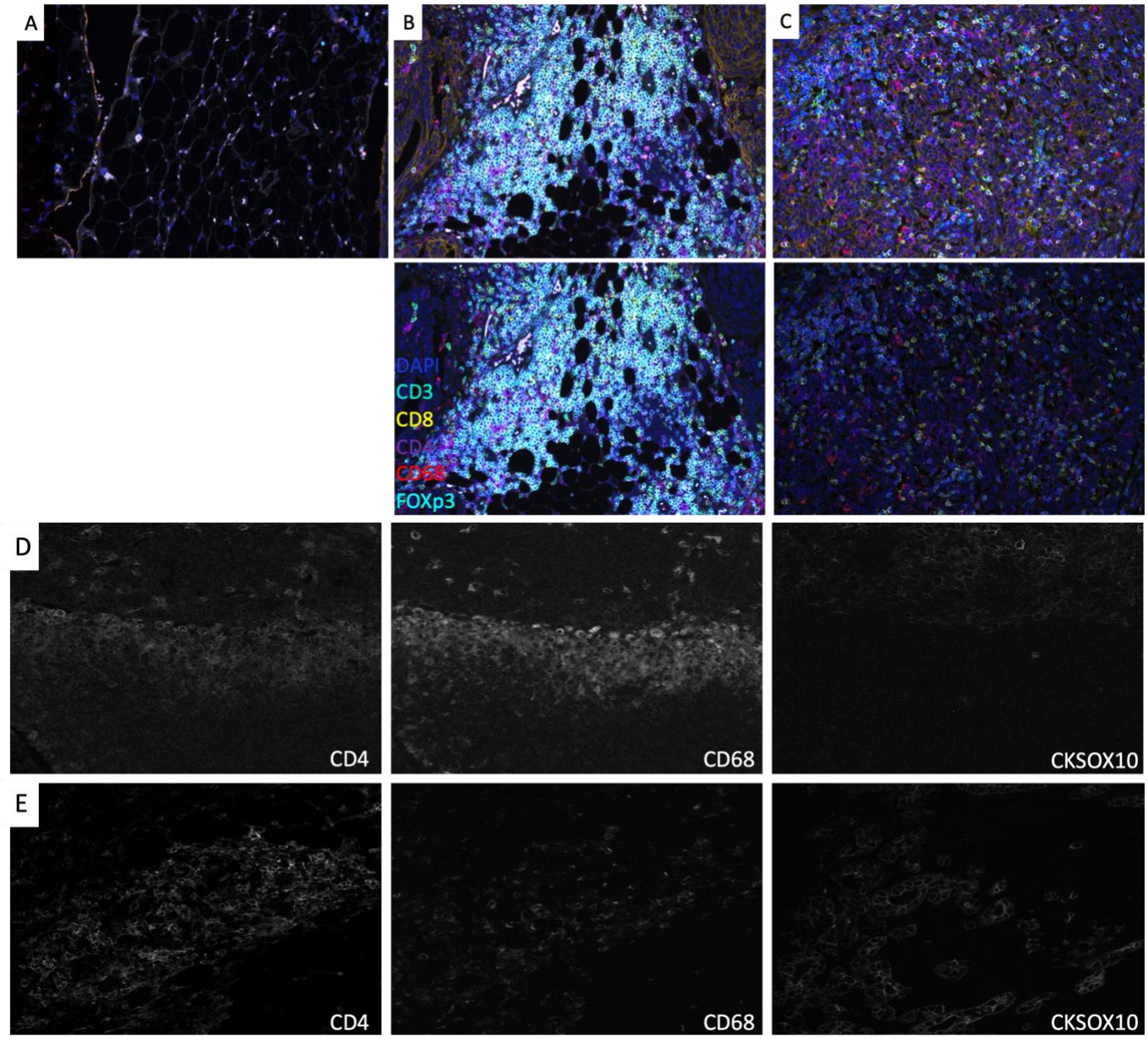

Figure 12. Immune infiltration of the omentum. The presence of CD4+, CD8+, Tregs and macrophages in **A)** normal omentum, **B)** NT metastatic omentum, and **C)** NACT metastatic omentum. **D)** Single channel staining of CD4, CD68, and CK-SOX10 of a NT primary tumour. **E)** Single channel staining of CD4, CD68, and CK-SOX10 of a NACT metastatic omentum. All images are 20X.

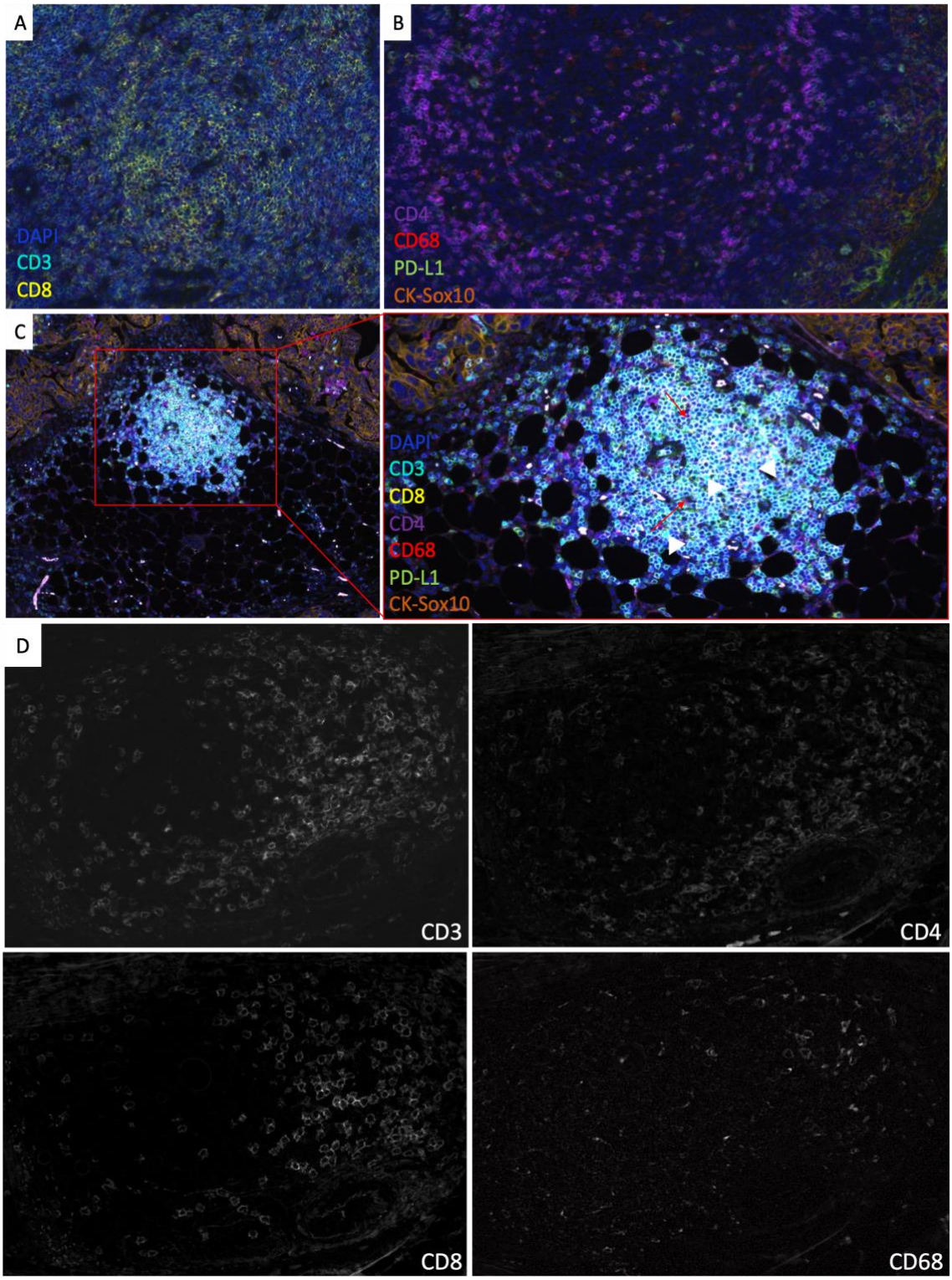

Figure 13. Comparison of tonsil tissue and suspected TLO/FALC in metastatic omentum. A and B) Within the tonsil tissue there were two distinct cellular distributions, one rich in CD8+ cells (A), and one formed by a layer of CD4+ cells and a few macrophages around a germinal centre (B) (magnification 20X). **C)** Regions of adipose tissue found in the metastatic tumour in this omental samples. These regions were enriched with CD3+CD4+ lymphocytes with a small amount of Tregs (white arrowheads) and macrophages (red arrows). These regions are suspected to be FALCs around which the metastatic tumour cells seed and begin invading the omentum, replacing the adipose tissue (5X magnification, zoom in at 20X). **D)** Single channel staining of CD3, CD4, CD8, and CD68 of a FALC in NACT omentum (20X magnification).

Treatment status	Patient ID	Omental sample	Ovarian sample
NT	SWBH163	✓	✓
	SWBH172	✓	✓
	SWBH174	✓	✓
	SWBH197	✓	
	SWBH249	✓	
	SWBH256		✓
NACT	SWBH187	✓	
	SWBH199	✓	
	SWBH237		✓
	SWBH239	✓	

Table 7. Summary of tissue sources and treatment statuses of FFPE patient samples.

3.2 Phenotype Profiles of ROIs Represent Marker Expression Quantification

There was a lower prevalence in CK-SOX10 in NACT omental samples when compared to NT samples (figure 14A) which could point to treatment efficacy in the respective patients. There is also an increased prevalence of CD4+ and CD3CD4+ cells in the NACT samples. This difference is also present when comparing the uninvolved omental tissues with the tumoural ROIs within the NT samples (figure 14B). In the NACT omental samples where available, the uninvolved tissues showed a decreased prevalence of CD4+ and CD3CD4+ cells, while there was increase in CD3CD4PD1+ cells specifically, as well as CD3CD8+ cells (figure 14C).

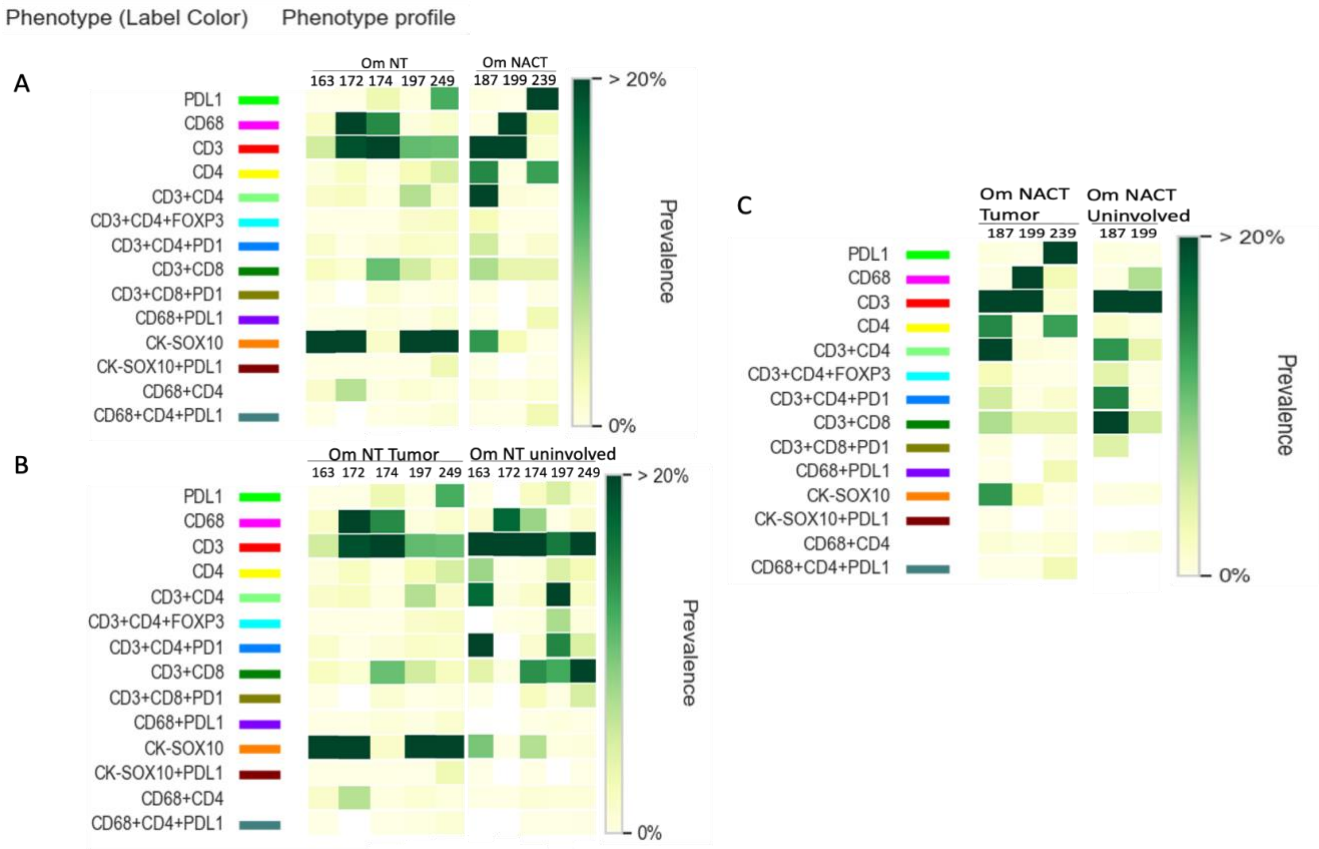

Figure 14. Phenotype profiles of omental FFPE samples. A) Prevalence expression of individual and combined markers in NT and NACT omental tumour samples. **B)** Comparison of NT tumoural vs uninvolved tissues from within the same patient samples (samples 163, 172, 174, 197, 249). **C)** Comparison of NACT tumoural vs uninvolved tissues from within the same patient samples where available (samples 187 and 199).

It should be noted that it is difficult to objectively compare the differences between the NT and NACT ovarian samples, as there was only one available NACT sample (SWBH237). However, we can still observe a visibly increased prevalence of CD68+, CD3+ and CD3CD8+ cells in the NT samples. CK-SOX10 appears to be similar, unlike the omental samples (figure 15A). Uninvolved NT ovarian ROIs seemingly showed decreased prevalence of CK-SOX10 as expected, and increased prevalence of CD3+ cells (SWBH256), CD3CD8+ and PDL1+ cells generally. Similarly, the NACT sample showed a higher prevalence for CD4+, CD3+, CD3CD8+, and CD3CD8PD1+ cells in uninvolved ROIs (figures 15B-C). Overall, it appears that the NT tumoural ROIs show a more similar immune infiltrate proportion to non-cancerous ovarian tissues.

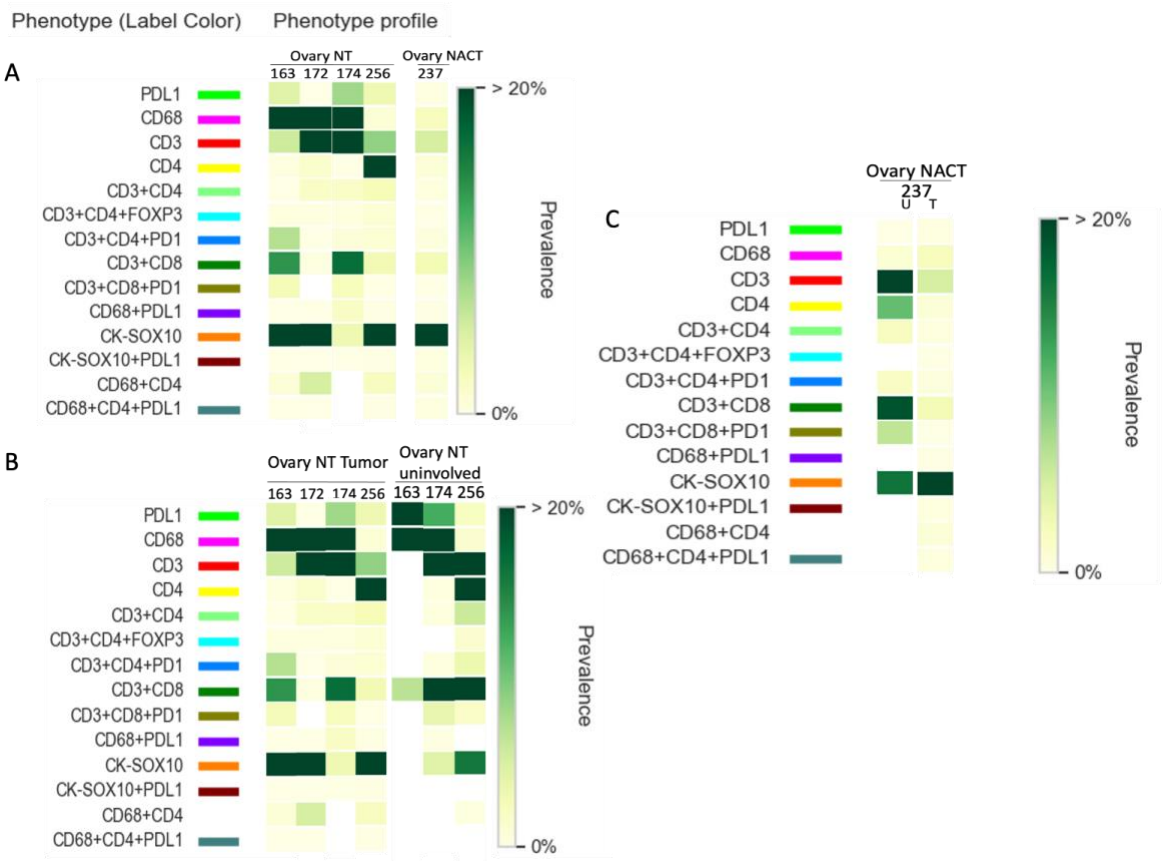

Figure 15. Phenotype profiles of ovarian FFPE samples. A) Prevalence expression of individual and combined markers in NT and NACT ovarian tumour samples. **B)** Comparison of NT tumoural vs uninvolved tissues from within the same patient samples (samples 163, 172, 174, 256). **C)** Comparison of NACT tumoural vs uninvolved tissues from within the same patient sample (sample 237).

3.3 t-SNE Supports Common Origins of Metastatic and Primary Tumours

Using t-SNE, we were able to collectively look at representative proportions of NT and NACT samples respectively and separate the different cellular phenotypes to determine if there are any similarities in between the omental and ovarian distributions of cancer cells and immune

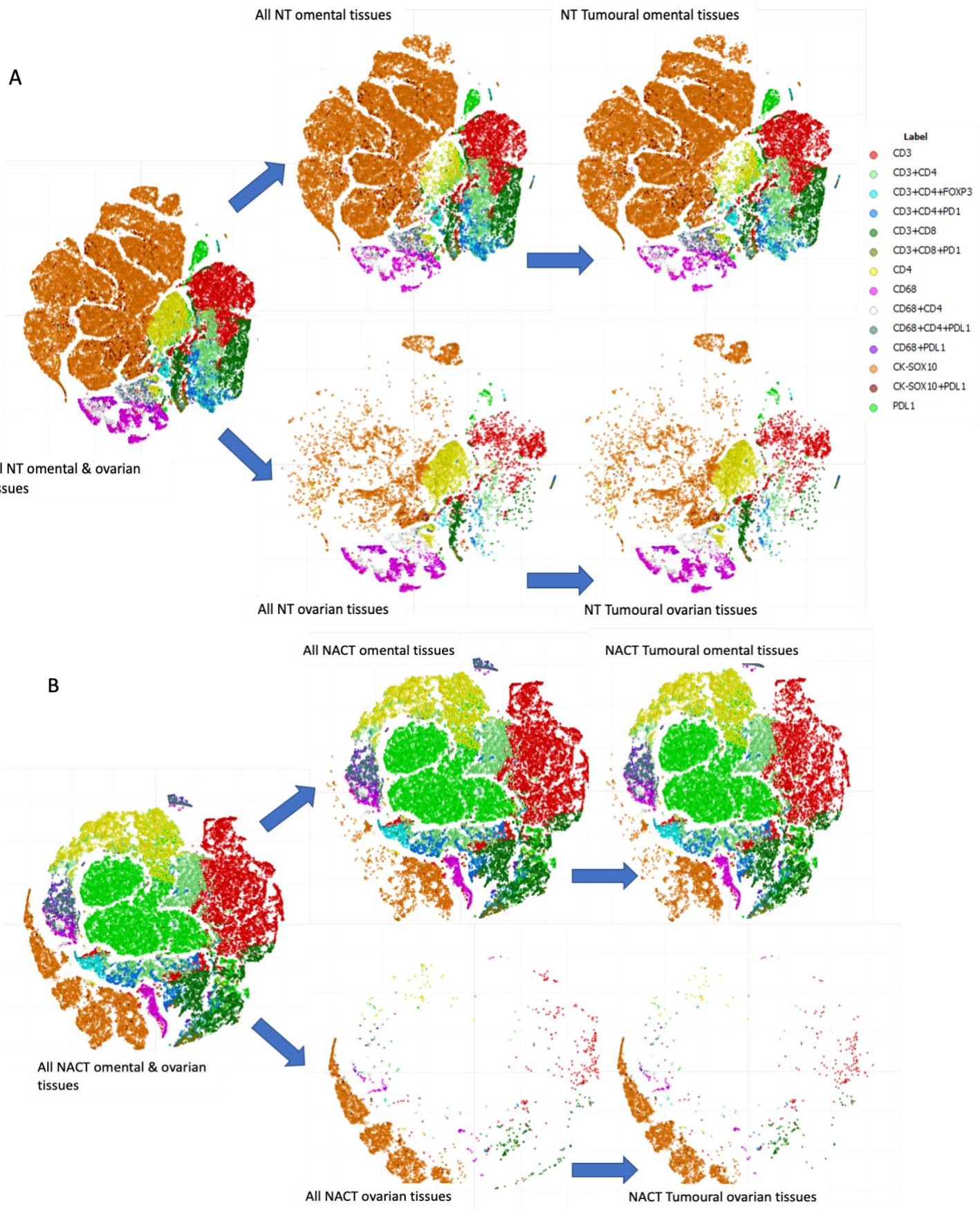

Figure 16. Cumulative and gated t-to SNE plots of NT and NACT samples. Samples are consolidated according to treatment status to look for and establish similarities in phenotypical characteristics of specific cells clusters. Gating is applied to separate ovarian and omental samples, and further gating isolates the cells from tumoural ROIs. A) NT samples. B) NACT samples.

infiltrates. When we observe the clusters of CK-SOX10+ cells (figure 16A), which denote cancerous cells in our cohort, we can see the spatial concordance between omental and ovarian tumoural cells, which supports the notion that the metastatic cells belong to the same origin as the primary tumours, particularly from the samples from which there were both omental and ovarian samples available to directly compare (SWBH163, 172 and 174). The similar distributions of lymphoid immune infiltrates also support the secondary tumours maintaining their phenotypes with metastasis before treatment. Interestingly, there is a population of CD68CD4PDL1+ macrophages which are found in the omentum that appear to be absent in the ovarian tumours. Additionally, in agreement with the phenotype profiles, there is a much smaller size of gross immune infiltrate and PDL1+ cells in the NACT ovarian sample, the majority of which are sequestered in the omental portion (figure 16B).

Notably, there are a few patients that displayed very similar t-SNE profiles for immune infiltrates and/or tumour cells. This suggests that despite patient-to-patient variability that can be observed in the clinic, there are patients that can be divided into subgroups that may predict how they respond to chemo- or immunotherapy (figure 17).

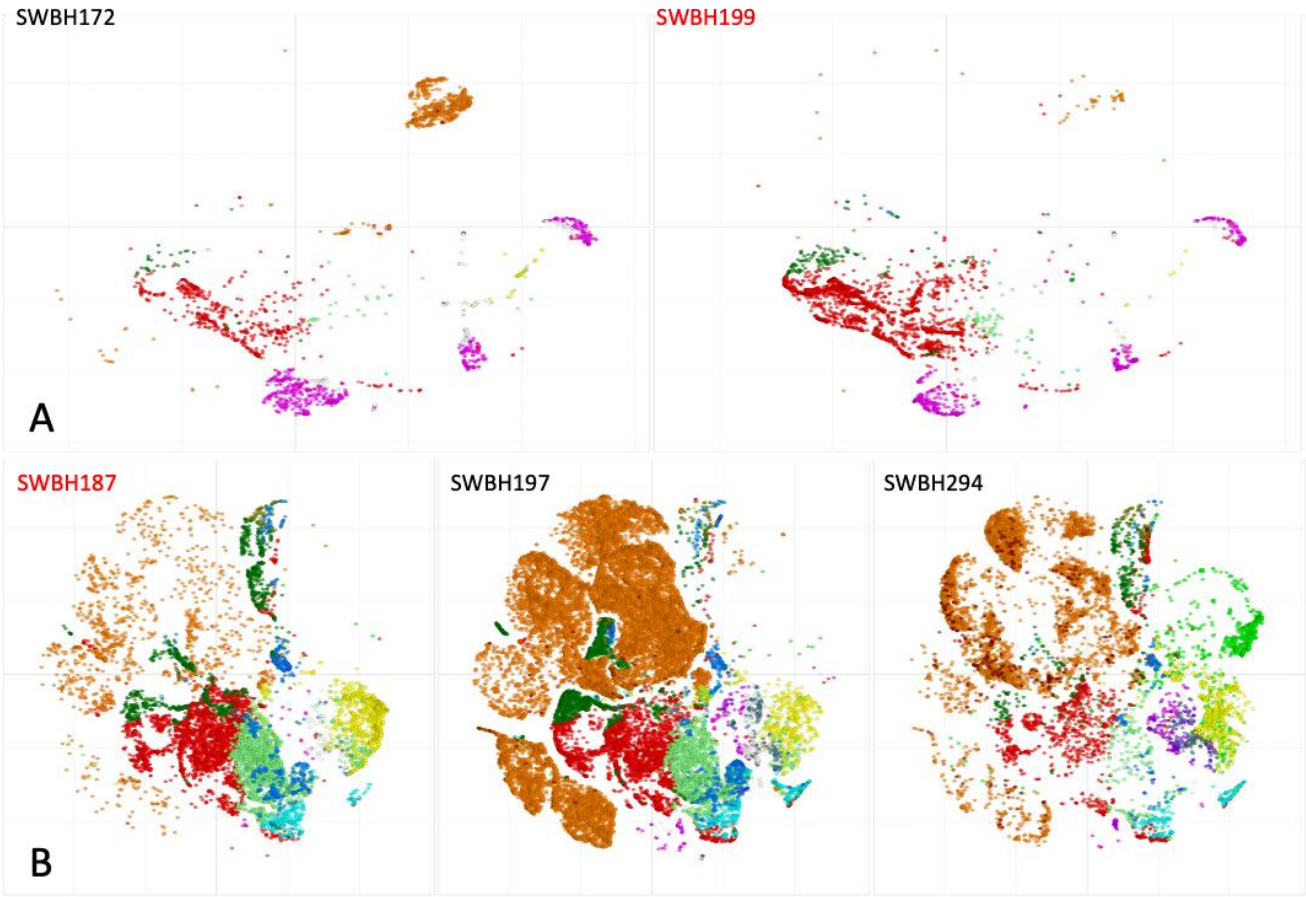

Figure 17. Omental patient samples that display similar phenotypic t-SNE distributions. A) NT SWBH172 and NACT SWBH199 display corresponding spatial coordinates for CD68+ macrophages, CD3+, CD3CD4+ and CD3CD8+ lymphocytes, and CK-SOX10 tumour cells. B) NT SWBH197 and SWBH294, and NACT SWBH187 match up in CD3+, CD4+, CD3CD4+, CD3CD4PD1+, CD3CD4FOXP3+, and CD3CD8+ lymphocytes, some CD68+ and CD68CD4+ macrophages, and CK-SOX10 tumour cells.

3.4 Comparing FC and IF Data of the Same Patient Population

To validate the quantification of the population proportions detected by the nuclear detection and phenotyping applications, the total number of relevant events from the 10 samples (CD4+, CD8+ and CD68+) were plotted against the corresponding population proportions previously obtained via FC data where possible (SWBH237 FC data was unavailable due to tissue allocation). Any variances in the means can be attributed to physical differences in the sample portions used for FFPE preparation and FC analysis respectively. Despite this, no statistically significant differences were seen, which can confirm that the FC and IF microscopy data are analogous and support each other (figure 18).

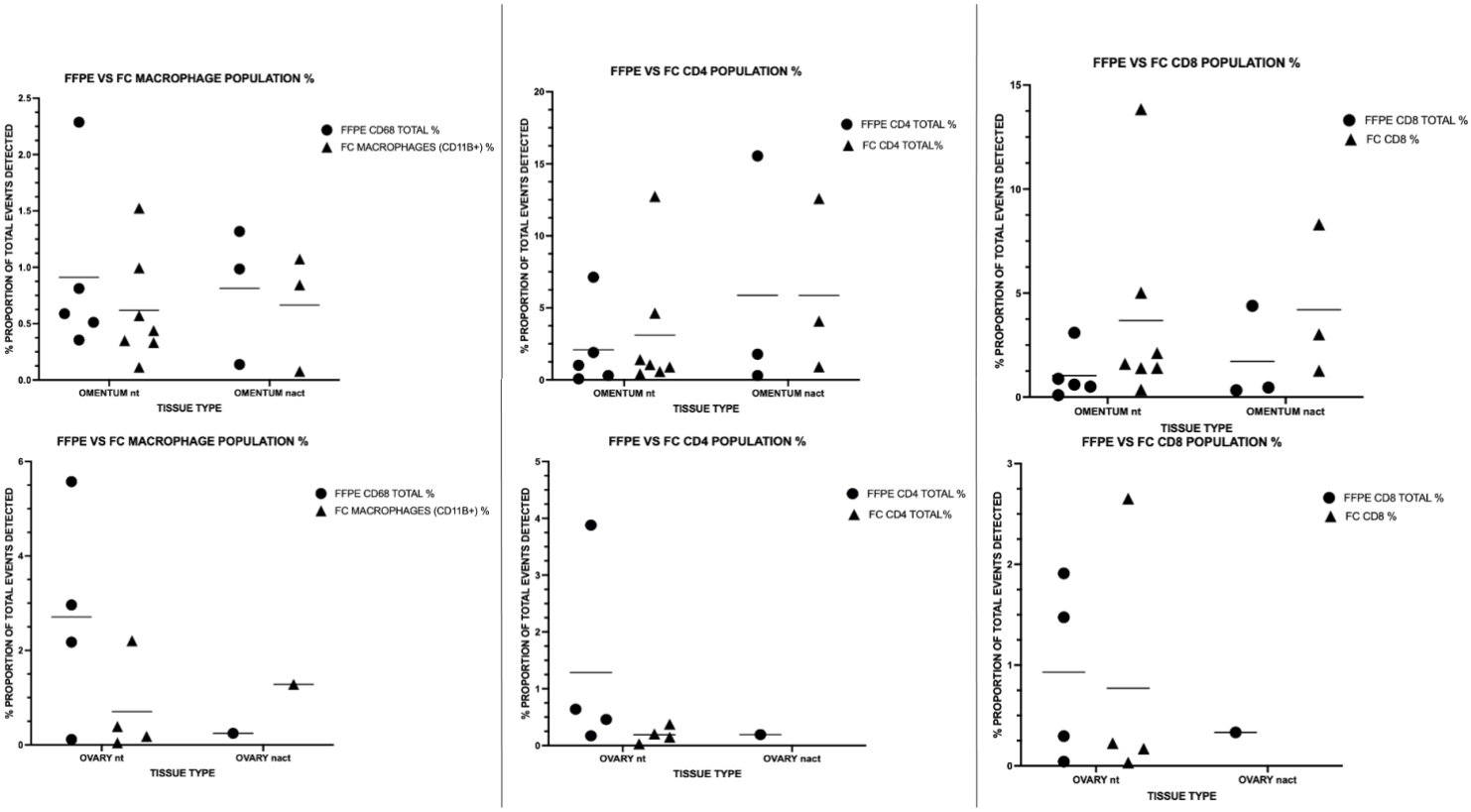

Figure 18. Quantitative comparison of cellular events detected by IF microscopy of FFPE samples and FC analysis of the same NT and NACT patient samples. Top row) omental samples. Bottom row) ovarian samples. No significant difference was found between population proportions of quantified FFPE and FC events where tests of significance were valid.

Discussion and Limitations

1. Discussion

1.1 DARE Mice May Favour a Higher Immune: Stromal Composition Than WT in TLOs

DARE mice are expected to have a larger number of stromal cells within the FALCs and lymph nodes, due to chronic inflammation and therefore an increased expression of TNF. However, what is observed in the data is a small but statistically significant reduction in the gross stromal population of omental stromal cells in DARE mice when compared to their WT littermates. It is also unclear why the IL-33 reporter mice, which should have similar internal conditions to the WT mice, have such varied differences in some stromal subpopulations, such as BECs and FRCs, when compared to both WT and DARE mice. Macrophage representation in DARE mice was significantly higher in both omental and mLN samples than in WT mice, and it would be of use in future work to confirm the phenotype of these macrophages, though they are most likely to be M1 pro-inflammatory macrophages. This, in addition to the markedly increased proportion of cDC2 in DARE omental tissues, supports the increased activation of CD8+ lymphocytes and their expression of IFNγ upon restimulation with PMA/Ionomycin, as well as CD4+ expression of IL-10. Conversely, mLN populations of CD8+ and CD4+ exhibited an increase in IFNγ and IL-10 expression respectively upon restimulation in WT samples, which may suggest some impairment of immune function in the mLNs of DARE mice.

1.2 Macrophages Play Varied Roles in Influencing FALC Immuno-Stromal Functions at Different Disease Stages

In human tissues, parallel to DARE mice, NACT omental samples in IF microscopy showed defined clusters of macrophages within the tumoural ROIs, which are likely to be locally expanded TAMs supporting anti-tumoural immune responses, likely to be M1 macrophages. Direct comparisons to normal omental tissues via IF microscopy was not feasible, we turned to FC data. Uninvolved, or normal, omental tissues were richer in M2 macrophages, as well as Tregs, indicating immunosuppressive environments. Similar M2:M1 proportions were seen in NT tumours, however, with a significantly larger population of M1/M2 macrophages and cDC2 cells, suggesting an increase in immune activity in NT environments compared to the uninvolved omentum. Previous unpublished data from our lab supports this, citing fold increases of CD4+ and CD8+ lymphocytes of 7.5 and 10.8 between normal and NT metastases respectively. On the other hand, the CD4+ and CD8+ lymphocytes were 7.8 and 7.44 times less respectively in NACT omentum compared to NT omentum, and there is no significant difference in CD69 and IFNγ expression across normal, NT or NACT tissues. As NACT leads to

changes in the distribution and proportions of the immune infiltrate in metastatic tumours, full mount microscopy would be useful to determine if and how the organization of FALCs is also affected and how that may affect the support of the tumour relating to the distribution of stromal subpopulations angiogenesis, extra-cellular matrix production, etc, as we were unable to visualise these changes with the limited IF microscopy panel.

To further examine the importance of the immune-stromal interactions in supporting the tumoural environment, a study by Opzoomer *et al*. [35] identified a specific Lyve-1+ TAM population that was complicit in the advancement of mammary adenocarcinoma in a murine breast cancer model by interacting directly with perivascular α-smooth muscle actin (αSMA+) CAFs in the perivascular niche (characterised by CD45-CD31-CD90+ profiles). PDGF-CC expressed by Lyve-1+ TAMs interacted with CAF-expressed PDGFRα and PDGFRβ. Another distinguishing property of this CAF subtype was the low expression of FAP and PDGFRα ($FAP^{lo}CD140a^{lo}$). In our study, FC data of stromal subpopulations characterised by CD45-CD235a-PDPN+/-CD31+/- were also examined for FAP and PDGFRα expression to ascertain which of the CD31- subtypes (FRCs and DNs) could most closely resemble the CAFs described by Opzoomer *et al.* As previously mentioned in the results, the cells closest to these CAFs in our study were found in the DN stromal subpopulation, which is the least characterised subpopulation in recent literature [15], and therefore, are a prime target for more characterisation and specialised identification, to further pinpoint their role in OvCa metastasis in the omentum.

1.3 Optimising IF microscopy Protocols as a Supplement to Broader Clinical Translation

IF microscopy and its analysis in VisioPharm has shown that its potential in classifying patients with similar phenotypic distributions of immune infiltrates and tumour deposits (figure 17), and it can perhaps be used as a predictive model to supplement initial screening in newly diagnosed and staged patients to determine if they would be suitable candidates for platinum-based, taxane-based chemotherapy, or more novel immunotherapies targeted towards their specific mechanisms of disease progression, be it immune checkpoint inhibitors, such as anti-CTLA-4, anti-PDL1, anti-PD1, intra-tumoural heterogeneity or otherwise [36]. This endeavour would benefit from more specific antibody panels and careful preparation of sample slides and demarcation of tumour borders to avoid contaminating the data with signals from cells outside the specified regions of interest. Supplementary screening using patient derived organoids (validated using FC and IHC microscopy to confirm presence of stromal-tumoural contact) can be used for *ex-vivo* therapeutic testing before progressing to

in-vivo experiments in controlled clinical trial settings. Generating 3D cultures of organoids from patient derived OvCa samples was possible in both non-adherent and Matrigel-based cultures (figure 19).

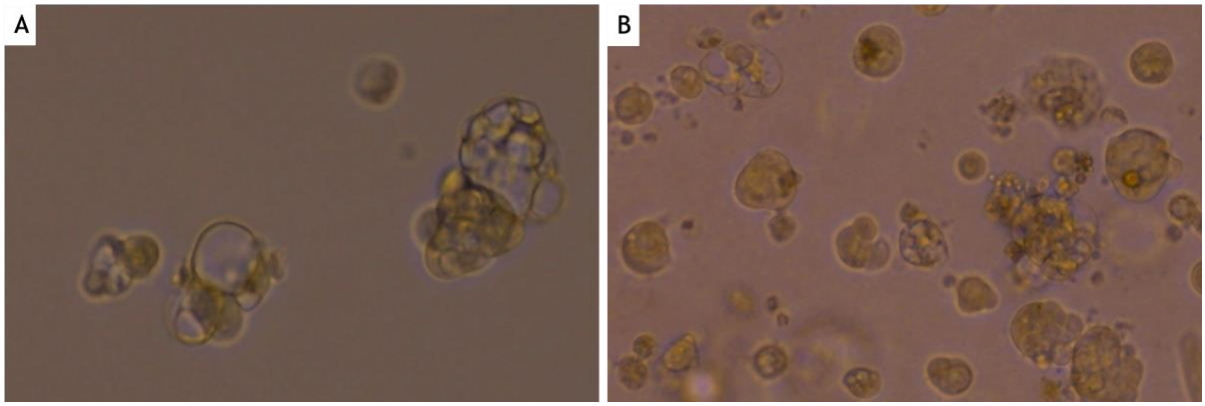

Figure 19. 3D patient derived OvCa organoids. A) Non-adherent culture. **B)** Matrigel-based culture. (Magnification at 20X).

In summary, we were able to show that the inflammatory state of DARE omental FALCs is like that of NT patients' omental environment, with increased cDC2s, M1/M2 macrophages, CD8+ and CD4+ T-cells. In addition, $FAP^{lo}CD140a^{lo}$ DN stromal cells were identified as a target for further characterization for their potential role in OvCa omental metastasis. We were also able to show that both NT and NACT patients could be classified into distinct phenotypic profiles, which in conjunction with FC, IF microscopy and biopsy-derived organoid models, could serve as predictors for personalized treatment and management routes in clinical medicine. Future work would include using FC to focus on the $FAP^{lo}CD140a^{lo}$ DN stromal cells to identify unique surface markers, and eventually collaborating with Ultivue on a more comprehensive and specified panel to identify other immune cells beyond CD3, CD4 and CD8 such as DCs and neutrophils, to further classify macrophages as M1, M2 or M1/M2 subtypes, and to detect stromal cells and their direct proximity to tumoural and immune cells within the primary and metastatic niches.

2. Limitations

Unfortunately, throughout the duration of the project, many difficulties, setbacks, and limitations impeded the potential progress that could have been achieved. The project had a rough start due to the COVID-19 pandemic and lockdowns, which greatly delayed necessary trainings, such as access to and use of the BMSU facility and FC unit for up to a year. Ineffective communication with the surgeon and his team resulted in inadequate sample collection, transport, and delivery, in addition to inaccessibility to pertinent prognostic patient information, such as staging and classification of cancer subtypes following debulking

surgeries, remission/relapse status, co-morbidities and other conditions that may have contributed to disease progression and patient-to-patient variability.

The IF staining and image acquisition also proved difficult in terms of preparing the slides from the FFPE blocks (high adiposity of the omental samples compromised the structural integrity of the tissues when transferring to the slides in a heat dependant process), staining the slides with a limited, pre-designed panel, and doubling the ovarian and omental samples from the same patients on the same slides in an attempt to minimize costs and avoid wasting costly reagents. Furthermore, the resulting image files retrieved from Ultivue were massive; this led to frequent crashing of the VisioPharm software and loss of data and analyses, which had to be repeated several times, over a span of several weeks each time. Contact with the VisioPharm support team allowed us to build custom cellular phenotype detection and characterisation apps to quantify and sort the different cell types in the samples, but we were still limited by the features of the program, and several planned analyses were not possible to conduct. Additionally, the pre-designed panel provided by Ultivue was initially designed for melanomas rather than ovarian cancers, and as such was limited. Markers for B cells, M1 and M2 macrophages, neutrophils and dendritic cells were not part of the panel, and should this work be repeated in the future, it would be prudent to incorporate them into the staining to better align the IF microscopy findings with those from the FC analyses.

On a different note, the personal struggles that arose during the project proved to be rather overwhelming and had long-term repercussions. I was diagnosed with several disabilities, as well as debilitating long COVID, which severely impacted my ability to engage with the programme, and support from the university was minimal. Despite an 8 month-long medical leave of absence, there is little to no improvement in my condition, and this has had a tangible effect on the quality and quantity of work I can produce. I can only hope that there is understanding regarding the difficult and tumultuous course that this project has taken.

References

1. Motohara, T., et al., *An evolving story of the metastatic voyage of ovarian cancer cells: cellular and molecular orchestration of the adipose-rich metastatic microenvironment.* Oncogene, 2019. **38**(16): p. 2885-2898.
2. Krishnan, V., et al., *In Vivo and Ex Vivo Approaches to Study Ovarian Cancer Metastatic Colonization of Milky Spot Structures in Peritoneal Adipose.* J Vis Exp, 2015(105): p. e52721.
3. Kuroki, L. and S.R. Guntupalli, *Treatment of epithelial ovarian cancer.* BMJ, 2020. **371**: p. m3773.
4. Eisenhauer, E.A., *Real-world evidence in the treatment of ovarian cancer.* Ann Oncol, 2017. **28**(suppl_8): p. viii61-viii65.
5. UK, C.R. *Ovarian Cancer Survival Statistics*. [cited 2022 June]; Available from: https://cancerresearchuk.org/health-professional/cancer-statistics/statistics-by-cancer-type/ovarian-cancer/survival#heading-Zero.
6. Yu, L., et al., *Significance of CD47 and Its Association With Tumor Immune Microenvironment Heterogeneity in Ovarian Cancer.* Front Immunol, 2021. **12**: p. 768115.
7. Liu, J., X. Geng, and Y. Li, *Milky spots: omental functional units and hotbeds for peritoneal cancer metastasis.* Tumour Biol, 2016. **37**(5): p. 5715-26.
8. Yin, M., et al., *Tumor-associated macrophages drive spheroid formation during early transcoelomic metastasis of ovarian cancer.* J Clin Invest, 2016. **126**(11): p. 4157-4173.
9. Koppe, M.J., et al., *Recent insights into the pathophysiology of omental metastases.* J Surg Oncol, 2014. **110**(6): p. 670-5.
10. Frasca, D. and B.B. Blomberg, *Adipose Tissue: A Tertiary Lymphoid Organ: Does It Change with Age?* Gerontology, 2020. **66**(2): p. 114-121.
11. Sautes-Fridman, C., et al., *Tertiary lymphoid structures in the era of cancer immunotherapy.* Nat Rev Cancer, 2019. **19**(6): p. 307-325.
12. Hiraoka, N., Y. Ino, and R. Yamazaki-Itoh, *Tertiary Lymphoid Organs in Cancer Tissues.* Front Immunol, 2016. **7**: p. 244.
13. Buechler, M.B., W. Fu, and S.J. Turley, *Fibroblast-macrophage reciprocal interactions in health, fibrosis, and cancer.* Immunity, 2021. **54**(5): p. 903-915.
14. Jackson-Jones, L.H., et al., *Stromal Cells Covering Omental Fat-Associated Lymphoid Clusters Trigger Formation of Neutrophil Aggregates to Capture Peritoneal Contaminants.* Immunity, 2020. **52**(4): p. 700-715 e6.
15. Zotes, T.M., et al., *PI3K p110delta is expressed by gp38(-)CD31(+) and gp38(+)CD31(+) spleen stromal cells and regulates their CCL19, CCL21, and LTbetaR mRNA levels.* PLoS One, 2013. **8**(8): p. e72960.
16. Lee, W., et al., *Neutrophils facilitate ovarian cancer premetastatic niche formation in the omentum.* J Exp Med, 2019. **216**(1): p. 176-194.
17. Sako, A., et al., *Vascular endothelial growth factor synthesis by human omental mesothelial cells is augmented by fibroblast growth factor-2: possible role of mesothelial cell on the development of peritoneal metastasis.* J Surg Res, 2003. **115**(1): p. 113-20.
18. Zakarya, R., V.M. Howell, and E.K. Colvin, *Modelling Epithelial Ovarian Cancer in Mice: Classical and Emerging Approaches.* Int J Mol Sci, 2020. **21**(13).
19. Keffer, J., et al., *Transgenic mice expressing human tumour necrosis factor: a predictive genetic model of arthritis.* EMBO J, 1991. **10**(13): p. 4025-31.
20. Benezech, C., et al., *Inflammation-induced formation of fat-associated lymphoid clusters.* Nat Immunol, 2015. **16**(8): p. 819-828.

21. Nanki, Y., et al., *Patient-derived ovarian cancer organoids capture the genomic profiles of primary tumours applicable for drug sensitivity and resistance testing.* Sci Rep, 2020. **10**(1): p. 12581.
22. Maenhoudt, N., et al., *Developing Organoids from Ovarian Cancer as Experimental and Preclinical Models.* Stem Cell Reports, 2020. **14**(4): p. 717-729.
23. Kontoyiannis, D., et al., *Impaired on/off regulation of TNF biosynthesis in mice lacking TNF AU-rich elements: implications for joint and gut-associated immunopathologies.* Immunity, 1999. **10**(3): p. 387-98.
24. Luo, Z., et al., *Tumor microenvironment: The culprit for ovarian cancer metastasis?* Cancer Lett, 2016. **377**(2): p. 174-82.
25. Etzerodt, A., et al., *Specific targeting of CD163(+) TAMs mobilizes inflammatory monocytes and promotes T cell-mediated tumor regression.* J Exp Med, 2019. **216**(10): p. 2394-2411.
26. Zhang, N., et al., *LYVE1+ macrophages of murine peritoneal mesothelium promote omentum-independent ovarian tumor growth.* J Exp Med, 2021. **218**(12).
27. Etzerodt, A., et al., *Tissue-resident macrophages in omentum promote metastatic spread of ovarian cancer.* J Exp Med, 2020. **217**(4).
28. Robinson-Smith, T.M., et al., *Macrophages mediate inflammation-enhanced metastasis of ovarian tumors in mice.* Cancer Res, 2007. **67**(12): p. 5708-16.
29. Liu, Y., Y. Xia, and C.H. Qiu, *Functions of CD169 positive macrophages in human diseases (Review).* Biomed Rep, 2021. **14**(2): p. 26.
30. Li, J.Q., et al., *Distinct patterns and prognostic values of tumor-infiltrating macrophages in hepatocellular carcinoma and gastric cancer.* J Transl Med, 2017. **15**(1): p. 37.
31. Wang, B., et al., *High CD204+ tumor-infiltrating macrophage density predicts a poor prognosis in patients with urothelial cell carcinoma of the bladder.* Oncotarget, 2015. **6**(24): p. 20204-14.
32. Topf, M.C., et al., *Loss of CD169(+) Subcapsular Macrophages during Metastatic Spread of Head and Neck Squamous Cell Carcinoma.* Otolaryngol Head Neck Surg, 2019. **161**(1): p. 67-73.
33. Louwe, P.A., et al., *Cell origin and niche availability dictate the capacity of peritoneal macrophages to colonize the cavity and omentum.* Immunology, 2022. **166**(4): p. 458-474.
34. Li, H., et al., *CircITGB6 promotes ovarian cancer cisplatin resistance by resetting tumor-associated macrophage polarization toward the M2 phenotype.* J Immunother Cancer, 2022. **10**(3).
35. Opzoomer, J.W., et al., *Macrophages orchestrate the expansion of a proangiogenic perivascular niche during cancer progression.* Sci Adv, 2021. **7**(45): p. eabg9518.
36. Morand, S., et al., *Ovarian Cancer Immunotherapy and Personalized Medicine.* Int J Mol Sci, 2021. **22**(12).